A displacement/damage controlled seismic design method for MRFs with concrete-filled steel tubular columns and composite beams

Serras, Dionisios N.; Skalomenos, Konstantinos A.; Hatzigeorgiou, George D.

DOI:
10.1016/j.soildyn.2021.106608

Document Version
Peer reviewed version

Citation for published version (Harvard):
Serras, DN, Skalomenos, KA & Hatzigeorgiou, GD 2021, 'A displacement/damage controlled seismic design method for MRFs with concrete-filled steel tubular columns and composite beams', *Soil Dynamics and Earthquake Engineering*, vol. 143, 106608. https://doi.org/10.1016/j.soildyn.2021.106608

A displacement/damage controlled seismic design method for MRFs with concrete-filled steel tubular columns and composite beams

Dionisios N. Serras[1], Konstantinos A. Skalomenos[2,*] and George D. Hatzigeorgiou[1]

[1]School of Science and Technology
Hellenic Open University
Patras, GR-26335, Greece

[2]Department of Civil Engineering, School of Engineering
University of Birmingham
Edgbaston, Birmingham, B15 2TT, United Kingdom

Abstract: A displacement/damage controlled (DDC) seismic design method for composite (steel/concrete) frames, consisting of circular concrete-filled steel tube (CFT) columns and composite beams (steel beams connected with concrete floor slabs) is developed in this study. The proposed seismic design method controls displacement and damage in a direct way for all seismic performance levels including the one near collapse. More specifically, through empirical expressions this method can estimate the inter-storey drift ratio (IDR) of a designed structure and evaluate the damage index (DI) of critical members for a given seismic intensity. A reduced number of design iterations is achieved while the computationally demanding non-linear time-history analysis can be avoided. The necessary empirical expressions of the design method are derived by means of statistical and sensitivity analysis of a large response databank consists of IDR and DI that cover all the way from elastic behavior to final global dynamic instability and collapse. This response databank is created by performing extensive parametric incremental dynamic analyses of many composite framed structures of the kind considered here under many seismic motions and different soil types. Design examples reveal that the DDC design method successfully estimates the targeted IDR for the desired seismic performance level as well as controls the DI in critical beam-to-column joints in order to avoid a soft-storey failure mechanism or partial loss of structure. Compared to all steel framed structures, the composite frames considered here exhibit a better seismic performance with beams and columns exhibiting a 20% lower DI. The low-damage performance of composite frames is mainly emphasized as the number of storeys increases, while both the IDR and DI tend to fall within lower performance levels than those of the corresponding all steel frames for the same seismic intensity.

Keywords: Composite Frames; CFT columns; Composite beams; Performance-based Seismic Design; Damage control

*Corresponding author: Dr Konstantinos Skalomenos, Email: k.skalomenos@bham.ac.uk

1. INTRODUCTION

Concrete-filled steel tube/moment resisting frames (CFT-MRFs) are high-performance seismic-resistant building structures that effectively combine the large ductility of steel tubes and confined infill concrete of CFT columns with the highly energy-dissipative beam-to-column connections of the MRF structural system [1-6]. This enables engineers to adopt smaller seismic design forces to satisfy the same ductility demands with the conventional structures, resulting in more economical structures with smaller cross-sections [7, 8]. In such seismic design approaches, methodologies that offer a direct control of damage at both the component-level (e.g., critical members) and global-level (e.g., storeys) are very important to evaluate the level of inelasticity expected in the structure for the various levels of seismic intensity as well as support the design of structures that can efficiently absorb the seismic loads at high intensity levels.

It is well known that in earthquake-resistant design of structures, some degree of damage in the structural members is accepted because the cost of a structure designed to remain elastic during a seismic event would be very high. The main performance objectives of current seismic design codes, such as the EC8 [9], are the provisions for life safety (strength checking) and immediate occupancy (deformation checking). During the last 30 years or so, performance-based seismic design (PBSD) methods have emerged [10, 11], which employ the concept of displacement or local damage control in conjunction with the strength requirements to increasing earthquake actions. Through specific performance levels, the acceptance limits for the inter-storey drift ratio (IDR) and/or the member ductility or plastic rotation of a structure should be satisfied for the various seismic intensity levels. According to the force-based design (FBD) methods (e.g., EC8 [9]), deformation requirements should always be checked at the final stage since strength requirements have been satisfied at the starting stage of the design. According to the displacement-based design (DBD) method [12-15], only strength requirements should be checked since deformation requirements are automatically satisfied. By combining the advantages of FBD and DBD methods, a recent PBSD method namely the hybrid force/displacement-based design (HFD) method estimates drift and ductility demands through a deformation-controlled behavior factor q (or strength reduction factor) [16-18]. On the basis of well-known damage indices (DI), a seismic design method called the direct damage-controlled design (DDCD) method has been recently developed for the seismic design of planar steel MRFs [19]. The method employs DI as the main design parameter and thus damage is controlled at the global and local level in a direct manner. A seismic design method, therefore, should deal with the deformation control (hence damage reduction) of both structural and non-structural components in a fashion that is familiar to engineers. This would be realistic if IDR and local damage are directly used as evaluation parameters within the preliminary design procedure of a structure and not only checked at the end of the design process through nonlinear time-history analysis. This is needed even

more for CFT-MRFs, where little systematic investigation on their seismic behavior has been carried out, and for which according to EC8 [9], the selection of seismic design forces and performance objectives for their preliminary design is based on those for steel structures, thereby ignoring the enhanced performance arising from the composite action of both concrete and steel materials [7, 8].

Within the framework of DBD, methods that aim to control damage have been proposed for reinforced concrete structures [20] but they are based on the assumption of single-degree-of-freedom systems as DBD method dictates. In general, methods have been proposed in regard to the deformation or damage evaluation and assessment of composite steel/concrete structures [21-23] but without explicitly taking into account design characteristics and properties of the structures in their damage evaluation process. Thus, a damage-controlled seismic design framework cannot be fully supported at the preliminary phase of the structural design. The above methods do not always describe in a direct way the stability (or strength) of the frame under seismic loads and most of them do not rigorously account for structural system behavior and can give misleading results, particularly when dealing with nonlinear behavior at the onset of structural instability [24, 25]. Recent research studies have been focused in quantifying the structural characteristics of composite structures or the seismic intensity of ground motions through empirical expressions for estimating the deformation and damage. For example, Skalomenos et al. (2015) [7] conducted an extensive study investigating the seismic inelastic behavior of regular planar CFT-MRFs with steel I beams and developed simple formulae for the direct estimation of seismic displacements and local ductility demands for those types of structures. Kamaris et al. (2016) [26] studied the seismic behavior of CFT-MRFs with steel I beams to quantify their damage through simple expressions, combining the most used DI of the literature for local damage with the characteristics of the frames. However, these researches have considered the displacement and the DI as evaluation parameters separately and not as a combination within a preliminary seismic design framework for any limit state.

In this paper a displacement/damage controlled (DDC) design method for the seismic design of plane CFT-MRFs with composite beams (steel IPE beams connected with concrete floor slabs) is established within the existing framework of current seismic design codes and guidelines. In order to establish the method, two extensive parametric studies are conducted by considering a large number of CFT-MRFs (48 of them) under 50 seismic motions for soil types B and D (25 for each soil type). The response of these frames is obtained by nonlinear dynamic analyses with the aid of RUAUMOKO analysis program [27] and a response databank is created. Thus, empirical expressions are developed to estimate the IDR and DI via a statistical analysis procedure and are used in the framework of a design flowchart. A further investigation is conducted by comparing results from the proposed expressions with those at performance levels defined in SEAOC [10, 28] and useful findings are obtained. Design examples are presented for illustration purposes and for demonstrating the advantages of the method. Generally, the main advantages of the proposed method are: i) dimensioning of the composite structural members so that displacement

and damage are controlled at various performance levels in a direct manner that does not require global analyses and thus, reduces the design iterations; and ii) damage control locally and/or globally is accomplished through simple parameters that quantify the strength and stiffness of the buildings, thus nonlinear time-history analysis for seismic performance assessment as in [19] is not required. Finally, the DDC based designs of a three-storey and six-storey composite frames are compared with the damage-controlled based design of the corresponding all steel frames at various performance levels [26]. The results indicate a lower DI for the members and a better control of displacements in the composites structures. The proposed expressions are generally satisfactory for the type of plane composite structures considered in this study founded in the associated soil types. The design method is promising and can be extended to other type of structures, structural systems and soil types with the same rationality.

2. DESCRIPTION AND DESIGN OF COMPOSITE STRUCTURES

A total of 48 regular composite plane moment resisting frames are investigated in-detail for soil types B and D, covering a wide range of structural characteristics, such as the number of stories (n_s) with values of 3, 6, 9, 12, 15 and 20, number of bays (n_b) equal to 3, yield steel stress (f_y) with values of 275 and 355 *MPa* and compressive concrete strength (f_c) with values of 30 and 50 *MPa*. The storey height and bay width of all frames are h = 3 *m* and b = 6 *m*, respectively. As shown in Fig. 1(a), the examined frames consist of circular concrete filled-steel tube (CFT) columns (Fig. 1(b)) and composite beams (steel beams connected with concrete floor slabs) of 15 *cm* thickness, as shown in Fig. 1(c). Further information about the calculation of the effective width of composite beam (b_{eff}) (Fig. 1(c)) can be found in Ref. [29].

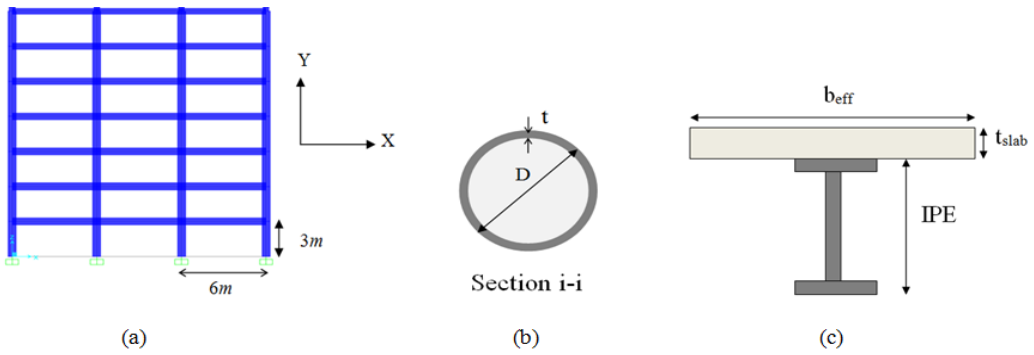

Figure 1: (a) A typical composite MRF, (b) circular CFT column section and (c) composite beam section (steel beam connected with concrete slab).

Capacity design considerations have been taken into account by satisfying at every joint the relation $\sum M_{RC} \geq 1.3 \cdot \sum M_{Rb}$, where $\sum M_{RC}$ and $\sum M_{Rb}$ are the sums of design values of the resistance moments of the columns and beams framing the joint, respectively. Tables 1 and 2 show the sectional

dimensions of the examined frames for soil types B and D, considering two values for the yield steel stress (275 and 355 *MPa*) and two values for the compressive concrete strength (30 and 50 *MPa*). Furthermore, values related to the number of stories n_s, the stiffness and strength ratios ρ, and α, respectively and the fundamental periods of vibration (T_1) are also included in Tables 1 and 2. The beam-to-column stiffness ratio ρ of a frame is defined at the story closest to the mid-height of the frame and calculated as [30]

$$\rho = \frac{\Sigma\left(I/l\right)_b}{\Sigma\left(I/l\right)_c} \tag{1}$$

where I, l_b and l_c are the second moment of inertia of members' section and the lengths of the beams (b) and columns (c), respectively. The column-to-beam strength ratio, a, is defined as [30]

$$a = \frac{M_{RC,1,av}}{M_{RB,av}} \tag{2}$$

where $M_{RC,1,av}$ is the average of the plastic moments of the columns resistance of the first storey and $M_{RB,av}$ is the average of the plastic moments of the beams resistance for all floors of the frame.

The frames under consideration are designed based on Eurocode-3 [31], Eurocode-4 [32] and Eurocode-8 [9] by using SAP2000 [33] and DEV-C++ [34]. The seismic load combination consists of the vertical load G + 0.5Q = 25 *kN/m* on the beams plus the earthquake load (E), whereas the gravity loads combination is 1.35G + 1.5Q = 42 *kN/m*. The dead loads (G) and the live loads (Q) of every floor are taken as 20 and 10 *kN/m*, respectively. Moreover, the design ground acceleration (a_g) and the behavior factor (q) are equal to 0.36g and 4.0, respectively for medium type structural ductility and Spectrum Type 1. Finally, the self-weight of beams and slabs is taken into consideration of the dead loads.

Table 1: Data for soil type B: Number of stories (n_s), sectional dimensional, column-to-beam strength ratio (a), beam-to-column stiffness ratio (ρ), and fundamental period of vibration (T_1).

No	n_s	Floors	CFT columns – material properties	Floors	Beams IPE	a	ρ	T_1
1	3	1-3	(406.4x6.30)-30-275	1-3	270	0.357	0.516	0.511
2	3	1-3	(406.4x6.30)-30-355	1-3	240	0.436	0.939	0.585
3	3	1-3	(406.4x6.30-50-275	1-3	270	0.339	1.359	0.518
4	3	1-3	(406.4x6.30)-50-355	1-3	240	0.432	0.996	0.563
5	6	1-2	(559x10.00)-30-275	1-2	330	0.450	1.000	0.865
		3-5	(406.4x6.30)-30-275	3-4	300			
				5	270			
		6	(355.6x6.00)-30-275	6	220			
6	6	1-2	(559x10.00)-30-355	1-2	270	0.644	0.500	1.065
		3-5	(406.4x6.30)-30-355	3-4	240			
				5	220			
		6	(355.6x6.00)-30-355	6	200			
7	6	1-2	(559x10.00)-50-275	1-2	360	0.445	1.577	0.872
		3-5	(406.4x6.30)-50-275	3-4	270			
				5	240			
		6	(355.6x6.00)-50-275	6	220			
8	6	1-2	(559x10.00)-50-355	1-2	270	0.637	0.669	1.017
		3-5	(406.4x6.30)-50-355	3-4	240			

				5	220			
		6	(355.6x6.00)-50-355	6	200			
9	9	1-4	(559x10.00)-30-275	1-3	400	0.255	0.926	1.243
				4	360			
		5-8	(406.4x6.30)-30-275	5-7	270			
				8	240			
		9	(355.6x6.00)-30-275	9	220			
10	9	1-4	(559x10.00)-30-355	1-3	300	0.383	0.498	1.529
				4	270			
		5-8	(406.4x6.30)-30-355	5-7	240			
				8	220			
		9	(355.6x6.00)-30-355	9	200			
11	9	1-4	(559x10.00)-50-275	1-3	400	0.252	1.010	1.203
				4	360			
		5-8	(406.4x6.30)-50-275	5-7	270			
				8	240			
		9	(355.6x6.00)-50-275	9	220			
12	9	1-4	(559x10.00)-50-355	1-3	300	0.380	0.541	1.456
				4	270			
		5-8	(406.4x6.30)-50-355	5-7	240			
				8	220			
		9	(355.6x6.00)-50-355	9	200			
13	12	1-7	(559x10.00)-30-275	1-4	400	0.898	0.990	1.478
				5-7	360			
		8-11	(406.4x6.30)-30-275	8-10	270			
				11	240			
		12	(355.6x6.00)-30-275	12	220			
14	12	1-7	(559x10.00)-30-355	1-4	330	0.247	0.519	1.866
				5-7	300			
		8-11	(406.4x6.30)-30-355	8-10	240			
				11	220			
		12	(355.6x6.00)-30-355	12	200			
15	12	1-7	(559x10.00)-50-275	1-4	400	0.178	1.010	1.486
				5-7	360			
		8-11	(406.4x6.30)-50-275	8-10	270			
				11	240			
		12	(355.6x6.00)-50-275	12	220			
16	12	1-7	(559x10.00)-50-355	1-4	330	0.243	0.576	1.772
				5-7	300			
		8-11	(406.4x6.30)-50-355	8-10	240			
				11	220			
		12	(355.6x6.00)-50-355	12	200			
17	15	1-4	(610x14.20)-30-275	1-2	550	1.095	1.021	1.537
				3-4	500			
		5-11	(559x10.00)-30-275	5-9	450			
				10	330			
				11	300			
		12-15	(406.4x6.30)-30-275	12-14	270			
				15	220			
18	15	1-4	(610x14.20)-30-355	1-4	360	0.262	0.456	2.098
		5-11	(559x10.00)-30-355	5-10	330			
				11	270			
		12-15	(406.4x6.30)-30-355	12-14	240			
				15	220			
19	15	1-4	(610x14.20)-50-275	1-2	550	0.151	1.119	1.505
				3-4	500			
		5-12	(559x10.00)-50-275	5-9	450			
				10	330			
				11-12	300			
		13-15	(406.4x6.30)-50-275	13-14	270			
				15	220			
20	15	1-4	(610x14.20)-50-355	1-4	360	0.257	0.518	1.977
		5-11	(559x10.00)-50-355	5-10	330			
				11	270			
		12-15	(406.4x6.30)-50-355	12-14	240			
				15	220			
21	20	1-10	(610x14.20)-30-275	1-5	600	0.090	1.178	1.828
				6-10	550			
		11-17	(559x10.00)-30-275	11-13	450			

				14-15	360			
				16-17	300			
		18-20	(406.4x6.30)-30-275	18-19	270			
				20	220			
22	20	1-10	(610x14.20)-30-355	1-5	500	0.133	0.637	2.342
				6-10	450			
		11-17	(406.4x6.30)-30-355	11-13	360			
				14-17	270			
		18-20	(406.4x6.30)-30-355	18-19	240			
				20	220			
23	20	1-10	(610x14.20)-50-275	1-5	600	0.087	1.398	1.769
				6-10	550			
		11-17	(559x10.00)-50-275	11-13	450			
				14-16	360			
				17	300			
		18-20	(406.4x6.30)-50-275	18-19	270			
				20	220			
24	20	1-10	(610x14.20)-50-355	1-5	500	0.127	0.765	2.163
				6-10	450			
		11-17	(559x10.00)-50-355	11-13	360			
				14-17	270			
		18-20	(406.4x6.30)-50-355	18-19	240			
				20	220			

Table 2: Data for soil type D: Number of stories (n_s), sectional dimensional, column-to-beam strength ratio (a), beam-to-column stiffness ratio (ρ), and fundamental period of vibration (T_1).

No	n_s	Floors	CFT columns – material properties	Floors	Beams IPE	a	ρ	T_1
1	3	1-3	(406.4x6.30)-30-275	1-3	270	0.356	1.307	0.511
2	3	1-3	(406.4x6.30)-30-355	1-3	270	0.358	1.207	0.546
3	3	1	(559x10.00)-50-275	1	300	0.949	0.770	0.431
		2-3	(406.4x6.30-50-275	2-3	270			
4	3	1	(559x10.00)-50-355	1	270	1.158	0.566	0.465
		2-3	(406.4x6.30)-50-355	2-3	240			
5	6	1-5	(559x10.00)-30-275	1-2	360	0.759	0.413	0.613
				3-4	330			
				5	300			
		6	(355.6x6.00)-30-275	6	240			
6	6	1-5	(559x10.00)-30-355	1-4	300	0.485	0.406	0.879
				5	270			
		6	(355.6x6.00)-30-355	6	220			
7	6	1-5	(559x10.00)-50-275	1-3	360	0.357	0.695	0.712
				4	330			
				5	300			
		6	(355.6x6.00)-50-275	6	240			
8	6	1-5	(559x10.00)-50-355	1-4	330	0.412	0.542	0.775
				5	270			
		6	(355.6x6.00)-50-355	6	220			
9	9	1-8	(559x10.00)-30-275	1-3	400	0.214	0.728	1.137
				4-6	360			
				7	330			
				8	300			
		9	(355.6x6.00)-30-275	9	240			
10	9	1-8	(559x10.00)-30-355	1-5	300	0.336	0.374	1.474
				6-7	270			
				8	240			
		9	(355.6x6.00)-30-355	9	220			
11	9	1-8	(559x10.00)-50-275	1-4	400	1.010	1.010	0.830
				5-6	360			
				7	330			
				8	300			
		9	(355.6x6.00)-50-275	9	240			
12	9	1-8	(559x10.00)-50-355	1-5	360	0.250	0.598	1.128
				6	300			

				7-8	270			
		9	(355.6x6.00)-50-355	9	220			
13	12	1-11	(559x10.00)-30-275	1-4	400	0.167	0.696	1.467
				5-7	360			
				8-10	330			
				11	270			
		12	(355.6x6.00)-30-275	12	220			
14	12	1-11	(559x10.00)-30-355	1-5	360	0.204	0.485	1.673
				6	330			
				7-8	300			
				9-10	270			
				11	240			
		12	(355.6x6.00)-30-355	12	220			
15	12	1-11	(559x10.00)-50-275	1-5	400	0.160	0.806	1.375
				5-8	360			
				9-10	330			
				11	270			
		12	(355.6x6.00)-50-275	12	240			
16	12	1-11	(559x10.00)-50-355	1-5	360	0.189	0.590	1.535
				6-8	330			
				9-10	300			
				11	240			
		12	(355.6x6.00)-50-355	12	220			
17	15	1-13	(610x14.20)-30-275	1-4	400	0.213	0.590	1.801
				5-10	360			
				11-12	330			
				13	300			
		14-15	(406.4x6.30)-30-275	14	270			
				15	220			
18	15	1-13	(610x14.20)-30-355	1-4	360	0.256	0.319	2.051
				5-10	330			
				11-12	300			
				13	270			
		14-15	(406.4x6.30)-30-355	14	240			
				15	220			
19	15	1-13	(610x14.20)-50-275	1-7	400	0.202	0.526	1.668
				8-10	360			
				11-12	330			
				13	300			
		14-15	(406.4x6.30)-50-275	14	270			
				15	220			
20	15	1-13	(610x14.20)-50-355	1-4	360	0.249	0.365	1.929
				5-10	330			
				11-12	300			
				13	270			
		14-15	(406.4x6.30)-50-355	14	240			
				15	220			
21	20	1-18	(610x14.20)-30-275	1-5	450	0.140	0.530	2.452
				6-11	400			
				12-15	360			
				16-17	330			
				18	300			
		19-20	(406.4x6.30)-30-275	19	270			
				20	220			
22	20	1-18	(610x14.20)-30-355	1-5	400	0.169	0.369	2.826
				6-11	360			
				12-15	330			
				16-17	300			
				18	270			
		19-20	(406.4x6.30)-30-355	19	240			
				20	220			
23	20	1-18	(610x14.20)-50-275	1-5	450	0.139	0.596	2.345
				6-11	400			
		19-20	(406.4x6.30)-50-275	12-15	360			
				16-17	330			
				18	300			
				19	270			
				20	220			
				20	220			

24	20	1-18	(610x14.20)-50-355	1-5	400	0.164	0.430	2.650
				6-11	360			
				12-15	330			
				16-17	300			
				18	270			
		19-20	(406.4x6.30)-50-355	19	240			
				20	220			

3. MODELING OF COMPOSITE FRAMES AND SEISMIC RESPONSE DATABASE

This section describes the modeling of circular CFT columns and composite beams of the examined frames based on the pertinent literature. In addition, a response databank is generated for soil types B and D, taking into account various ground motions compatible with those of soil types.

3.1 Modeling of the examined composite frames

The circular CFT columns are modeled based on the Refs. [35-40], while the composite beams according to Eurocode-4 [32]. The inelastic cycle behavior of circular CFT columns is simulated using the Ramberg-Osgood model as proposed by Serras et al. (2016) [36], while the composite beam is simulated utilizing the Al-Bermani hysteretic model [38]. The Ramberg-Osgood model describes the force-displacement hysteresis curve (F–d) displaying an elastic branch up to the yield displacement d_y and the corresponding yield force F_y, followed by a transition curve which leads to a plastic state, as shown in Fig. 2(a). The transition between the elastic and plastic branch, is controlled by the Ramberg-Osgood factor *r* whose influence is shown in Fig. 2(b). The factor *r* is computed by employing the associated expression in [36]. For the composite beams, the Al-Bermani model provides a smooth transition between the elastic and the inelastic regime for the force-displacement (F–d) relation while maintaining simplicity. This bounding-surface model is shown in Fig. 2(c) and requires five parameters to describe the F–d relation. These parameters are: the initial stiffness, k_o, the bounding stiffness, k_p ($k_p = p \cdot k_o$), the yielding force F_y and the coefficients alpha (α) and beta (β), which influence the bounding surface of the model as shown in Fig. 2(c). In this study both α and β parameters are set equal to zero, while the parameter *p* of the bounding stiffness is set equal to 0.02. In general, columns and beams are modeled with lumped plasticity elements defining the plastic hinges at their two ends. It should also be mentioned that beams can only deform in vertical bending due to the diaphragm action at each floor.

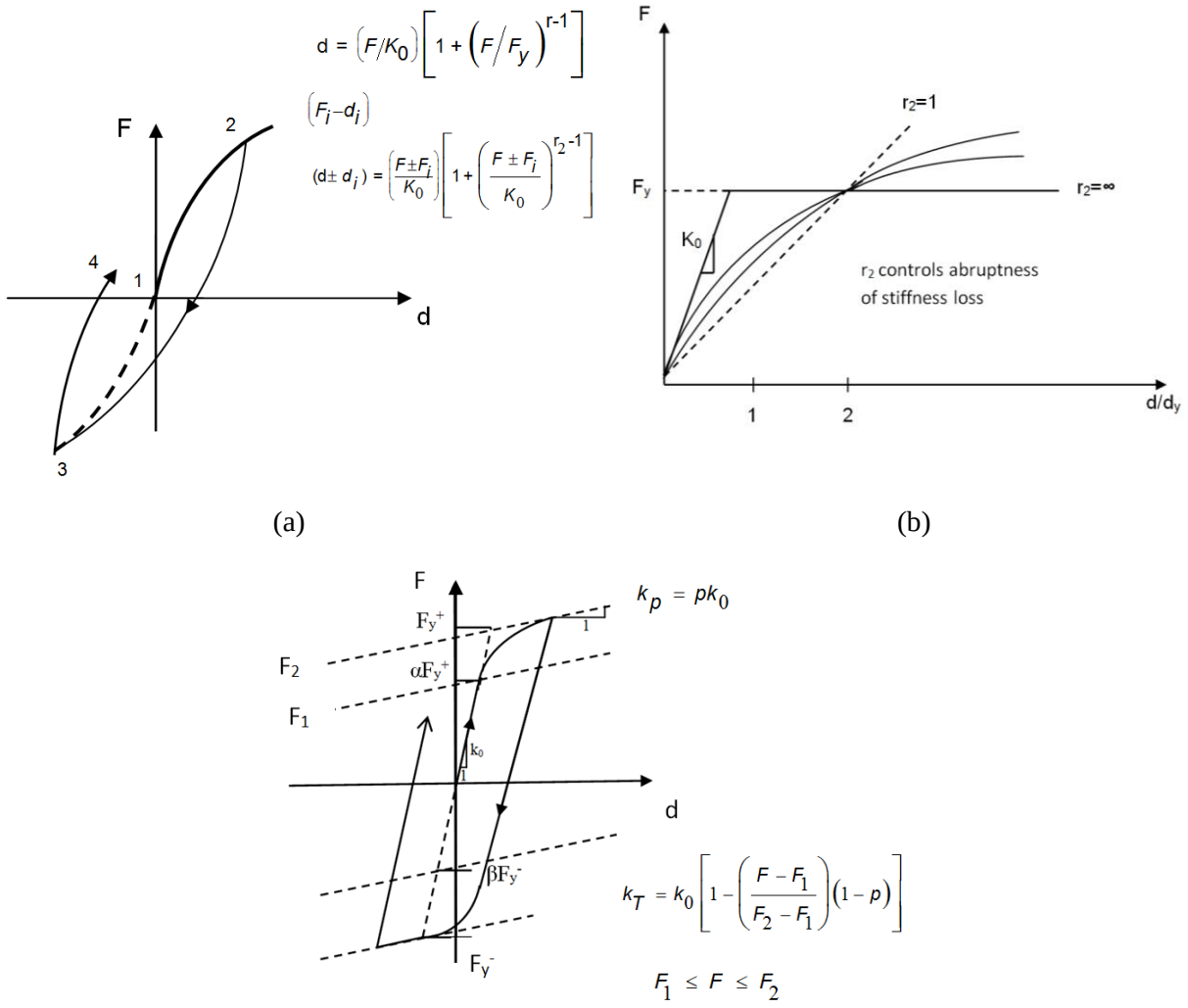

Figure 2: Ramberg-Osgood hysteretic model for circular CFT columns [36]: (a) force-displacement relation and (b) factor *r*. Al-Bermani hysteretic model for composite beams: (c) force-displacement relation

3.2 Ground motions and seismic response of frames

The examined (48) frames, described in section 2, are subjected to a set of 50 artificial accelerograms (25 for each examined soil type) compatible with the Eurocode 8 [9] spectrum, as shown in Fig. 3. Their seismic response is determined using the RUAUMOKO analysis program [27] by performing non-linear dynamic analyses via Newmark's constant average acceleration method. Stiffness and mass proportional damping is assumed with proportionality factors for the stiffness and mass matrices, respectively, as a result of assumed 3.0% viscous damping in the first and second modes [7]. The damping matrix is based on a Raleigh damping model and use the stiffness of the structure at the beginning of the time-history [41]. Thus, a response databank is generated by thousands of dynamic nonlinear time history analyses

using appropriate scale factors (*SFs*) to drive the frames to the desired damage levels of the various performance levels. Each ground motion is scaled to several intensity levels designed to force the structure all the way from elastic behavior to final global dynamic instability and collapse. These analyses are based on incremental dynamic analysis (IDA).

As shown in Fig. 3(a), the values of the periods (*T*) of many frames in Table 1, belong to the branch C-D because they are greater than 0.5 (0.5 < T < 2.0). However, there are two frames (i.e. twenty storey frames) where the values of their periods are greater than 2.0 (T > 2.0). On the other hand, on the basis of Fig. 3(b), the frames of Table 2 ranging from three stories to six stories belong to the branch B'-C' because 0.20 < T < 0.80, whereas frames ranging from six stories to fifteen stories belong to the branch C'-D' (0.80 < T < 2.0). In addition, it can be observed that the values of the periods for twenty storey buildings are greater than 2.0 (T > 2.0). Finally, it should be noted that artificial ground motions were selected in order to avoid the use of high scale factors in IDA as well as to secure that the code limitation for the range of compatibility periods (i.e., $0.2T_1$ to $2.0T_1$) is satisfied for each analyzed structure.

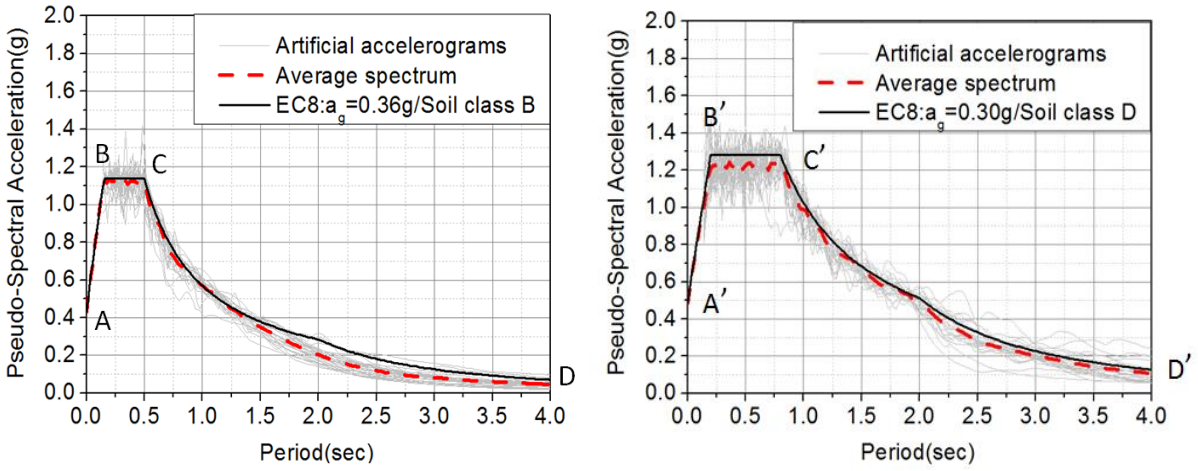

Figure 3: Acceleration response spectra of 50 seismic artificial earthquakes for the soil types B and D (25 seismic artificial earthquakes for every soil type) compatible with the Eurocode-8 [9].

4. EXPRESSIONS FOR INTERSTOREY DRIFT RATIOS AND DAMAGE INDICES

In order to estimate the inter-storey drift ratios (IDR) and damage indices (DI) of the composite plane frames considered in this study, empirical equations are proposed in this section obtained by regression analysis of the response databank. The reliability of the proposed equations is verified via the correlation coefficient (R^2), expressing the central tendency and the dispersion of the error introduced by the proposed relations and calculated as the ratio of the 'approximate' value from the expressions to the 'exact' dynamic inelastic analysis value of *R* i.e. R_{app}/R_{exact}. At this stage, it should be mentioned that the

results of the proposed relations and dynamic inelastic analyses are denoted by the words 'approximate' values and 'exact' values, respectively.

4.1 Expressions for IDR as a function of structural and ground motion characteristics

Performing regression analysis and sensitivity analysis on the whole response databank, the target IDR (IDR_t) for a predefined performance level can be expressed in terms of the pseudo-spectral acceleration $S_a(T)$ in g (g is the gravity acceleration) at the fundamental period T in *sec* of the designed structure, the storey number (n_s), the column-to-beam strength ratio a, the beam-to-column stiffness ratio ρ, the yield steel stress f_y in *MPa* and the compressive strength of the concrete f_c in *MPa*.

Equations (3) – (11) provide expressions for the IDR_t and soil types B and D for the cases of including parameters a (column-to-beam strength ratio) and ρ (beam-to-column stiffness ratio) and ignoring these parameters, respectively, while Tables 3 and 4 show the corresponding values of the constants k_i for every proposed equation. These tables also provide the values of the correlation coefficient R^2 as well as the range of IDR for which each proposed equation is valid. This range has been defined by optimizing the regression analysis within various ranges of IDR. As one can observe, the R^2 coefficients for Eqs (3) – (11) indicate that in case the building frame has not been designed as yet, and hence parameters a and ρ are not known, Eqs (6) and (7) can be used within an acceptable level of confidence. The only parameter requiring calculation is the period T by using code defined simple expressions. However, much simpler expressions for IDR_t are also provided (i.e. Eq. (5)) for a rapid estimation without the need of a period T calculation. R^2 in this case is lower. Eqs (3) – (7) refer to soil type B, while Eqs (8) – (11) refer to soil type D. It is noted that five expressions are proposed for the soil type B and four for the soil type D. This is due to the fact that the sensitivity analysis showed a negligible improvement of R^2 when both the T and n_s were taken into account for the development of the expression for the soil type D.

$$IDR_t = \left(a^{k_1} \cdot \rho^{k_2} \cdot \left(\frac{f_c}{20} \right)^{k_3} \cdot \left(\frac{f_y}{235} \right)^{k_4} \cdot S_a(T)^{k_5} \cdot T^{k_6} \right) \cdot k_7 \quad (3)$$

$$IDR_t = \left(a^{k_1} \cdot \rho^{k_2} \cdot \left(\frac{f_c}{20} \right)^{k_3} \cdot \left(\frac{f_y}{235} \right)^{k_4} \cdot S_a(T)^{k_5} \cdot n_s^{k_6} \right) \cdot k_7 \quad (4)$$

$$IDR_t = \left(\left(\frac{f_c}{20} \right)^{k_1} \cdot \left(\frac{f_y}{235} \right)^{k_2} \cdot S_a(T)^{k3} \cdot T^{k_4} \cdot n_s^{k_5} \right) \cdot k_6 \quad (5)$$

$$IDR_t = \left(\left(\frac{f_c}{20} \right)^{k_1} \cdot \left(\frac{f_y}{235} \right)^{k_2} \cdot S_a(T)^{k3} \cdot T^{k_4} \right) \cdot k_5 \quad (6)$$

Table 3: Parameters (k_i) and correlation coefficient (R^2) of Eqs (3) – (6) for soil type B.

n_s	*Eqs*	R^2	*IDR*	k_1	k_2	k_3	k_4	k_5	k_6	k_7	k_8
	(3)	76.92%	≤ 3.2%	-0.1227	-0.2141	-0.1411	0.6543	1.3450	0.9021	0.0541	
	(4)	75.75%	> 3.2%	-0.1039	-0.3169	-0.1497	1.1380	1.2560	0.5852	0.0234	
	(5)	76.43%	≤ 3.2%	-0.1102	0.2290	1.3810	1.8930	-0.6176	0.1381		
	(6)	75.92%	> 3.2%	-0.1713	0.9018	1.3300	0.9996	0.0618			

$$IDR_t = \left(a^{k1} \cdot \rho^{k2} \cdot \left(\frac{f_c}{20} \right)^{k3} \cdot \left(\frac{f_y}{235} \right)^{k4} \cdot S_a(T)^{k5} \cdot T^{k6} \right) \cdot k_7 \quad (7)$$

$$IDR_t = \left(a^{k1} \cdot \rho^{k2} \cdot \left(\frac{f_c}{20} \right)^{k3} \cdot \left(\frac{f_y}{235} \right)^{k4} \cdot S_a(T)^{k5} \cdot n_s^{k6} \right) \cdot k_7 \quad (8)$$

$$IDR_t = \left(\left(\frac{f_c}{20} \right)^{k1} \cdot \left(\frac{f_y}{235} \right)^{k2} \cdot S_a(T)^{k3} \cdot n_s^{k4} \right) \cdot k_5 \quad (9)$$

$$IDR_t = \left(\left(\frac{f_c}{20} \right)^{k1} \cdot \left(\frac{f_y}{235} \right)^{k2} \cdot S_a(T)^{k3} \cdot T^{k4} \right) \cdot k_5 \quad (10)$$

Table 4: Parameters (k_i) and correlation coefficient (R^2) of Eqs (8) – (11) for soil type D.

n_s	*Eqs*	R^2	*IDR*	k_1	k_2	k_3	k_4	k_5	k_6	k_7	K_8
=3 and ≤ 20	(7)	78.81%	≤ 1.8%	0.9504	1.2780	-0.1305	0.6700	1.0980	2.0750	0.0632	
	(8)	74.07%	> 1.8%	0.7690	1.1740	-0.5095	1.5610	0.9302	1.4920	0.0043	
	(9)	71.48%	> 1.8%	-0.2528	0.4149	0.8520	0.5054	0.0136			
	(10)	74.06%	≤ 1.8%	-0.1221	0.1080	0.9368	0.6875	0.02343			

Based on Tables 3 and 4, it can be seen that every proposed equation for soil types B and D are established depending on the IDR. Fig. 4 shows indicative scatters where the results of the proposed method are compared with those obtained by dynamic analysis, using a detailed statistical investigation. For this reason, the 16% and 84% confidence levels corresponding to the median plus/minus one standard deviation give also the uncertainties associated with the seismic records. Examining Fig. 4(a) and 4(b) it is found that the dispersion generally varies due to the fact that the data corresponding to inter-storey drift ratio cover a wide range of multistorey buildings. In addition, for the proposed equations, which involve the parameters a and ρ, dispersion is observed to be large. Nevertheless, their accuracy is found to be satisfactory for design purposes despite the fact that during the analyses of the examined structures, the scatter behavior of results is unavoidable because of the uncertainties associated with the ground motions [42, 43].

a)

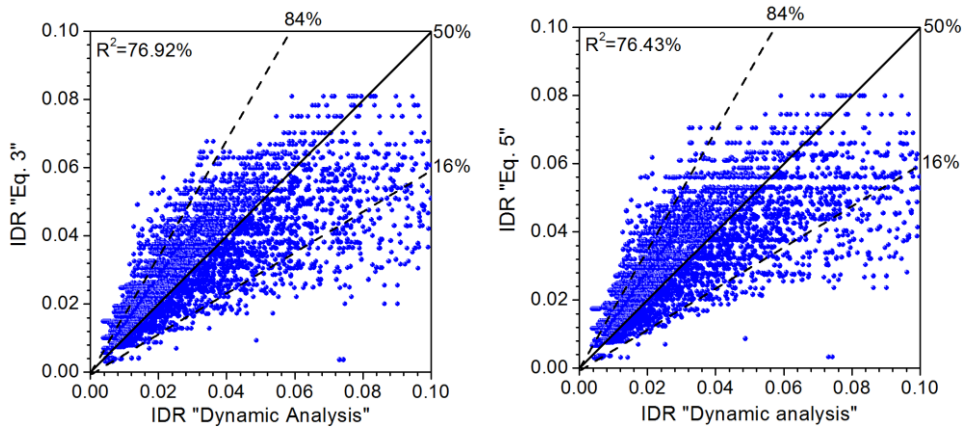

b)

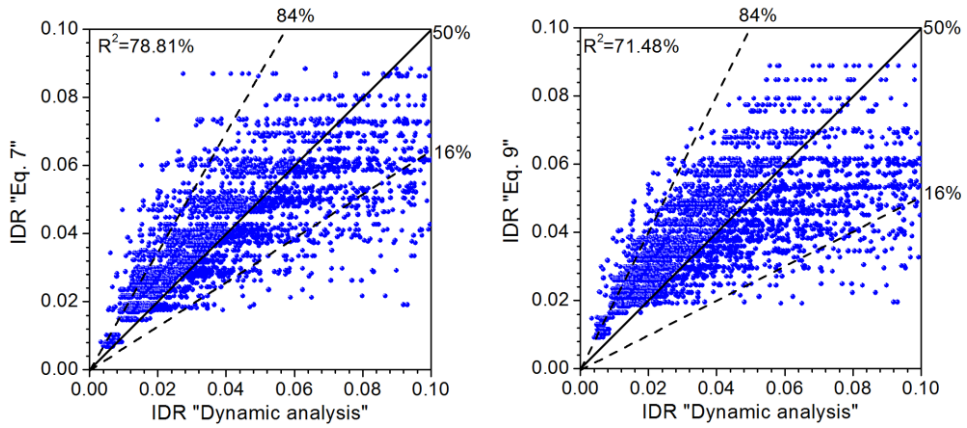

Figure 4: Maximum inter-storey drift ratio using (i.e., Eq. (3) and Eq. (7)) and ignoring a and ρ parameters (i.e., Eq. (5) and Eq. (9)): Proposed equations versus values obtained by "dynamic analysis" for: (a) soil type B and (b) soil type D.

4.2 Expressions for DI as a function of structural and ground motion characteristics

In this section, the Park-Ang damage index [44] is selected as the seismic damage measure due to its rationality and stability. This damage index takes into consideration both the maximum deformation and the hysteretic energy of dissipation of structural members and is defined as

$$DI = \frac{\mu_m}{\mu_u} + \frac{bE_h}{F_y \mu_u \delta_y} \tag{11}$$

where μ_m is the maximum ductility of the element, μ_u is its ultimate ductility and b represents a model constant parameter (usually, b=0.025-0.20) to control strength deterioration, E_h is the hysteretic energy absorbed by the element during the earthquake, F_y is the yield action of the element and δ_y is the yield displacement of the element. For steel and reinforced concrete structures the parameter b is equal to 0.025 [45] and 0.050 [46], respectively. In this research study, parameter b is set equal to 0.030 [26].

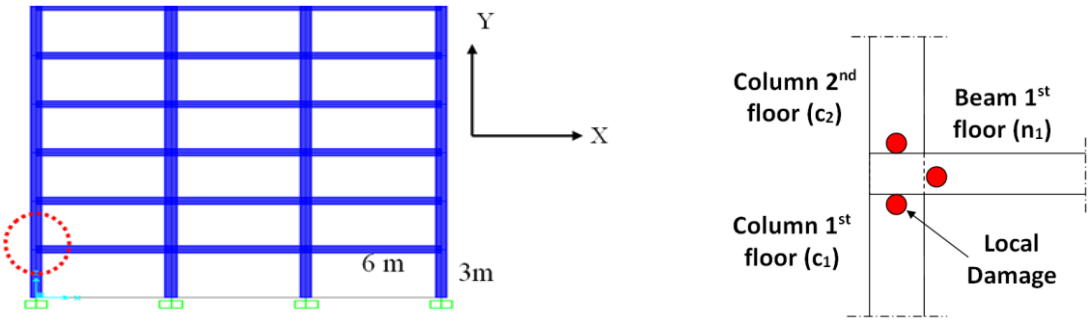

(a) (b)

Figure 5: (a) Typical composite building frame and (b) beam-to-column joints of 1st floor with damage points.

The following expressions for the damage indices in the forms $D^{(c_1)}$, $D^{(c_2)}$ and $D^{(n_1)}$ refer to the three points c_1, c_2 and n_1 at the beam-to-column joint of the first floor (Fig. 5) and they are given in terms of various structural parameters as defined in a previous section. Here, the parameter N is the ratio between the axial applied load N_{st} to the maximum axial strength N_{max}, i.e. $N = N_{st} / N_{max}$. The parameter N_{st} is derived from the seismic load combination, while the N_{max} is obtained by the axial force-bending moment interaction curve. Further information regarding the computation of N_{max} can be found in Refs [36, 37]. Thus, one has the following damage index expressions at the three joint points c_1, c_2 and n_1 of Fig. 5 as well as their constant parameters (k_i) in Tables 5 and 6. For completeness reasons, the correlation coefficient (R^2) of every proposed expression is also provided in those Tables. More specifically, Eqs (12) – (17) refer to soil type B with Eqs (15) – (17) ignoring a and ρ parameters.

$$D^{(c_1)} = \left(a^{k_1} \cdot \rho^{k_2} \cdot N^{k_3} \cdot IDR^{k_4} \cdot n_s^{k_5} \cdot S_a(T)^{k_6} \right) \cdot k_7 \tag{12}$$

$$D^{(c_2)} = \left(a^{k_1} \cdot \rho^{k_2} \cdot N^{k_3} \cdot IDR^{k_4} \cdot n_s^{k_5} \cdot S_a(T)^{k_6} \right) \cdot k_7 \tag{13}$$

$$D^{(n_1)} = \left(a^{k_1} \cdot \rho^{k_2} \cdot \left(\frac{f_c}{20} \right)^{k_3} \cdot \left(\frac{f_y}{235} \right)^{k_4} \cdot IDR^{k_5} \cdot n_s^{k_6} \cdot S_a(T)^{k_7} \right) \cdot k_8 \tag{14}$$

or

$$D^{(c_1)} = \left(\left(\frac{f_c}{20} \right)^{k_1} \cdot \left(\frac{f_y}{235} \right)^{k_2} \cdot T^{k_3} \cdot n_s^{k_4} \cdot S_a(T)^{k_5} \right) \cdot k_6 \tag{15}$$

$$D^{(c_2)} = \left(\left(\frac{f_c}{20} \right)^{k_1} \cdot \left(\frac{f_y}{235} \right)^{k_2} \cdot T^{k_3} \cdot n_s^{k_4} \cdot S_a(T)^{k_5} \right) \cdot k_6 \tag{16}$$

$$D^{(n_1)} = \left(\left(\frac{f_c}{20} \right)^{k_1} \cdot \left(\frac{f_y}{235} \right)^{k_2} \cdot T^{k_3} \cdot n_s^{k_4} \cdot S_a(T)^{k_5} \right) \cdot k_6 \quad (17)$$

Table 5: Parameters (k_i) and correlation coefficient (R^2) of Eqs (12) – (17) for soil type B.

n_s	*Eqs*	R^2	k_1	k_2	k_3	k_4	k_5	k_6	k_7	k_8
=3 and ≤ 20	(12)	77.63%	-0.5517	0.0106	0.5504	0.2177	-0.8252	0.3863	2.8690	
	(13)	76.44%	-0.1217	0.1660	0.4831	0.5725	-0.5338	0.1200	13.5100	
	(14)	70.64%	-0.0574	0.0438	0.09833	0.04475	0.2331	0.05580	0.4996	1.9058
	(15)	70.60%	0.0098	0.4690	-3.2793	2.0230	0.6034	0.0031		
	(16)	59.03%	-0.0695	0.0011	-0.0670	0.3111	0.8616	0.1260		
	(17)	66.58%	0.1182	0.2217	0.2601	0.0675	0.7954	0.3360		

Similar expressions for the case of soil type D have also been developed and are given by Eqs (18) – (23) as follows:

$$D^{(c_1)} = \left(a^{k_1} \cdot \rho^{k_2} \cdot N^{k_3} \cdot IDR^{k_4} \cdot n_s^{k_5} \cdot S_a(T)^{k_6} \right) \cdot k_7 \quad (18)$$

$$D^{(c_2)} = \left(a^{k_1} \cdot \rho^{k_2} \cdot N^{k_3} \cdot IDR^{k_4} \cdot n_s^{k_5} \cdot S_a(T)^{k_6} \right) \cdot k_7 \quad (19)$$

$$D^{(n_1)} = \left(a^{k_1} \cdot \rho^{k_2} \cdot \left(\frac{f_c}{20} \right)^{k_3} \cdot \left(\frac{f_y}{235} \right)^{k_4} \cdot IDR^{k_5} \cdot n_s^{k_6} \cdot S_a(T)^{k_7} \right) \cdot k_8 \quad (20)$$

or

$$D^{(c_1)} = \left(\left(\frac{f_c}{20} \right)^{k_1} \cdot \left(\frac{f_y}{235} \right)^{k_2} \cdot T^{k_3} \cdot n_s^{k_4} \cdot S_a(T)^{k_5} \right) \cdot k_6 \quad (21)$$

$$D^{(c_2)} = \left(\left(\frac{f_c}{20} \right)^{k_1} \cdot \left(\frac{f_y}{235} \right)^{k_2} \cdot T^{k_3} \cdot n_s^{k_4} \cdot S_a(T)^{k_5} \right) \cdot k_6 \quad (22)$$

$$D^{(n_1)} = \left(\left(\frac{f_c}{20} \right)^{k_1} \cdot \left(\frac{f_y}{235} \right)^{k_2} \cdot T^{k_3} \cdot n_s^{k_4} \cdot S_a(T)^{k_5} \right) \cdot k_6 \quad (23)$$

Table 6: Parameters (k_i) and correlation coefficient (R^2) of Eqs (18) – (23) for soil type D.

n_s	*Eqs*	R^2	k_1	k_2	k_3	k_4	k_5	k_6	k_7	k_8
=3 and ≤ 20	(18)	82.02%	0.5320	0.7199	0.7156	0.5029	-0.5503	-0.0997	43.1850	
	(19)	80.82%	0.9564	0.9043	0.5337	0.7778	0.1384	-0.1968	46.2100	
	(20)	72.87%	-0.0574	0.0438	0.0983	0.0447	0.2331	0.0558	0.4996	1.9058
	(21)	75.44%	-0.1006	-1.9727	5.0407	-4.4660	0.6571	782.051		
	(22)	58.92%	0.7343	-1.8735	3.6202	-2.9280	0.7005	25.092		
	(23)	66.55%	0.2759	-1.0843	1.5371	-0.9326	0.6297	3.3690		

According to the values of correlation factor (R^2), one can observe that the proposed relations are more accurate when the parameters a and ρ are taken into consideration. The proposed relations which ignore the parameters a and ρ provide also a good estimation of the damage indices of the examined members when the structure has not been designed yet. Additionally, Fig. 6 depicts the scattering for damage indices including the effect of a and ρ for the soil types B and D, adopting the same procedure as mentioned in subsection 4.1. In general, it can be seen that the damage indices of the first floor are lower than those of the second floor. On the other hand, it is observed that the damage indices of the composite beams are higher than those of the columns, satisfying the weak beam-strong column capacity design rule according to EC8 [9].

a)

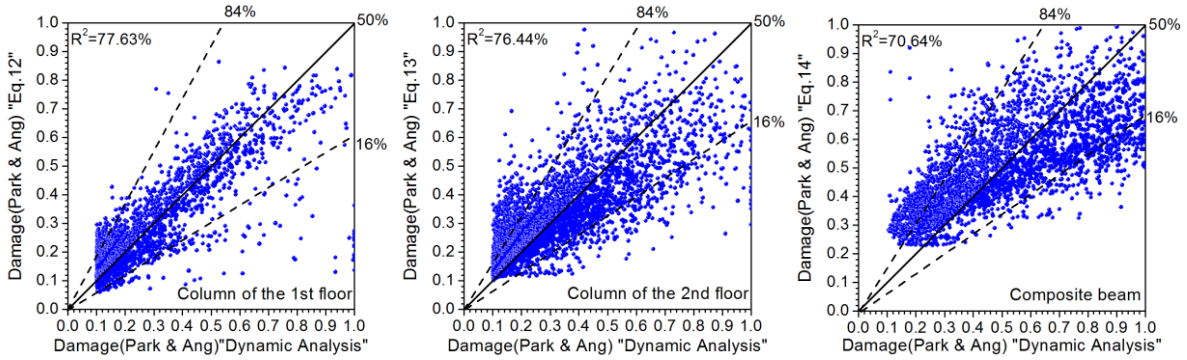

b)

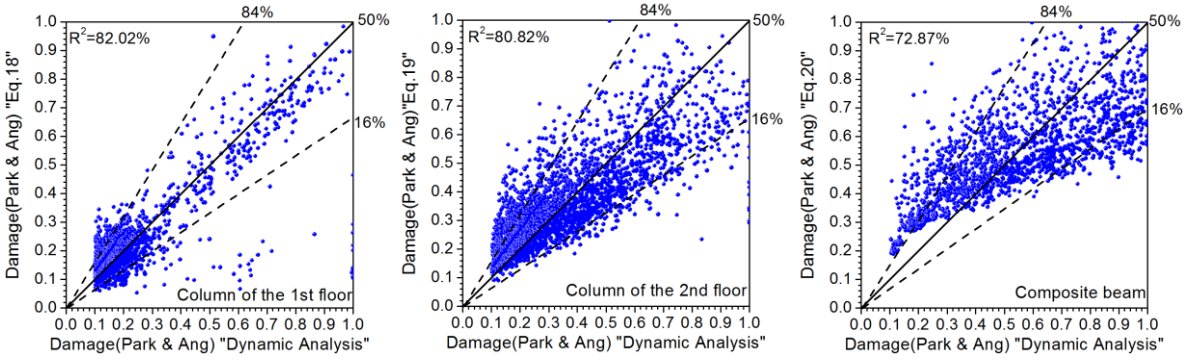

Figure 6: Structural damage indices of composite members: Proposed equations versus values obtained by "dynamic analysis" for: (a) soil type B and (b) soil type D.

5. VERIFICATION OF THE PROPOSED DESIGN EXPRESSIONS

In this section, two planar composite frames, which are different from those in the parametric study, are investigated in-detail for soil types B and D. Based on these two examples, the proposed relations are verified and established for such type of structures.

5.1 Description and design of the examined frames

A five-storey three-bay and a ten-storey three-bay composite frames founded on soil types D and B, respectively, are designed. Their bay width and storey height are equal to 5.0 *m* and 3.0 *m*, respectively. The steel yield stress (f_y) and concrete compressive strength (f_c) are assumed to be 235 and 40 *MPa*, respectively. As shown in Fig. 5(b), the joint of interest of the examined frames consists of two circular CFT columns and one composite (steel/concrete) beam consisting of a IPE section connected to a concrete slab of thickness equal to 15 *cm* (Fig. 1(c)).

The frames under consideration are designed according to Eurocode-3 [31], Eurocode-4 [32] and Eurocode-8 [9] by using SAP2000 [33] and DEV-C++ [34]. The seismic load combination consists of the vertical load G+0.5Q=25 *kN/m* plus the seismic load. The dead loads (*G*) and live loads (*Q*) of every floor are taken to be equal to 20 *kN/m* and 10 *kN/m* respectively, while the self-weight of beams and slabs is included in the dead loads. Additionally, the design ground acceleration (a_g) is assumed to be 0.36*g* and 0.30*g* for soil types B (10-storey frame) and D (5-storey frame) respectively, whereas the behavior factor is taken as 4.0. Table 7 shows the geometric properties of the examined frames along with their period *T*, the $S_a(T)$ and parameters *a* and ρ.

Table 7: Soil types, number of stories (n_s), geometric and material properties of the members, column to-beam strength ratio (*a*), beam-to-column stiffness ratio (ρ) and fundamental period of vibration (*T*).

Soil types	n_s	Floors	CFT columns dimensions – material properties	Floors	Beams IPE	*a*	ρ	*T* (sec)	$S_a(T)$ (g)
B	10	1-7	(406.4x6.30)-40-235	1-3	300	0.130	1.793	1.521	0.374
				4-6	270				
				7	240				
		8-10	(355.6x6.00)-40-235	8	240				
				9-10	220				
D	5	1-2	(457x8.00)-40-235	1	270	0.456	0.987	0.760	1.067
				2	240				
		3-4	(406.4x6.30)-40-235	3	240				
				4	220				
		5	(355.6x6.00)-40-235	5	200				

5.2 Application of the proposed design expressions

Each frame is subjected now to seven artificial accelerograms to perform an incremental nonlinear time-history (NLTH) analyses using RUAUMOKO analysis program [27]. In particular, seven artificial accelerograms are scaled to cover the entire range of structural response, from elasticity, to yielding and finally to global dynamic instability, as shown in Fig. 7. Four target inter-storey drift ratios are chosen randomly (i.e. 2.0%, 3.%, 4.0% and 5.0% for soil type B and 3.0%, 4.5%, 5.5% and 6.5 for soil type D), covering a wide range of the spectral acceleration $S_a(T_1)$ versus IDR curve and compared with those of

proposed relations. Table 8 presents the values of IDR_{TH} as obtained by the time-history analysis and the proposed relations for soil types B and D. In this Table, the $S_a(T_1)$ value of each IDR_{TH} is also provided. Finally, local damage indices DI of structural members at exterior joints like that of Fig. 5(b) are investigated in-detail for various IDR, taking into account and ignoring a and ρ parameters. Thus, Fig. 8(a) and Fig. 8(b) depict the level of damage in various members for various performance levels [10, 28] as obtained by NLTH analysis [27] and the proposed expressions (Eqs (12) – (23)).

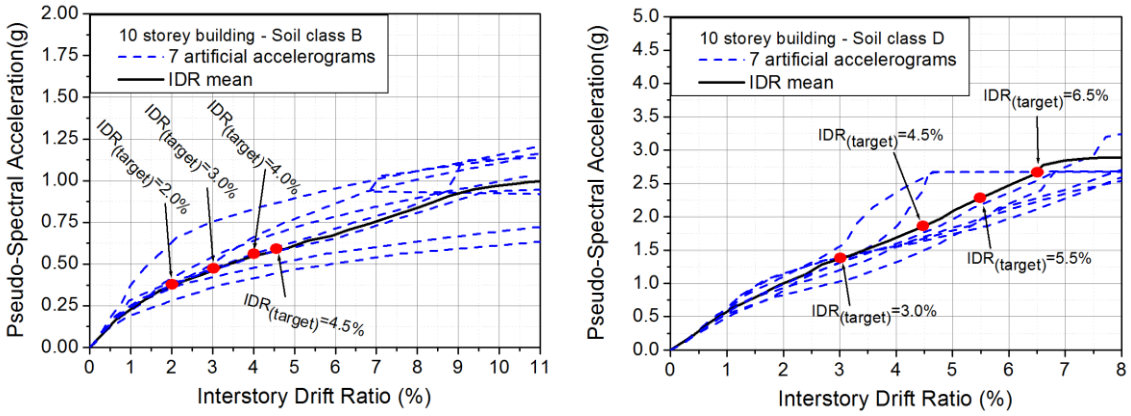

(a) (b)

Figure 7: (a) 10-storey building: IDA curve ($S_a(T)$ versus IDR) and (b) 5-storey building: IDA curve ($S_a(T)$ versus IDR) showing also various IDR_t.

Table 8: Soil types B and D: Number of stories (n_s), inter-storey drift ratio given by time-history analysis versus inter-storey drift ratio given by the proposed equations, using and ignoring a and ρ parameters.

Soil types	n_s	$S_a(T)$ (g)	IDR_{TH} (%) (Time history)	Eq. depending on a and ρ parameters				Eq. independent on a and ρ parameters			
				IDR(%) - Eq. (3)	Error (%) - (Eq. (3))	IDR(%) - Eq. (4)	Error (%) - (Eq. (4))	IDR(%) – Eq. (5)	Error (%) - (Eq. (5))	IDR(%) – Eq. (6)	Error (%) - (Eq. (6))
B	10	0.37	2.0	2.16	+7.40	-	-	1.75	-12.50	-	-
		0.46	3.0	2.92	-2.74	-	-	2.41	-24.48	-	-
		0.55	4.0	-[*a]	-	4.02	+0.49	-	-	3.79	-5.54
		0.59	4.5	-	-	4.27	-5.38	-	-	4.20	-7.14
		$S_a(T)$ (g)	IDR_{TH} (%) (Time history)	IDR(%) - Eq. (7)	Error (%) - (Eq. (7))	IDR(%) - Eq. (8)	Error (%) - (Eq. (8))	IDR(%) – Eq. (9)		Error (%) - (Eq. (9))	
D	5	1.30	3.0	3.13	+4.15	-	-	3.21		+6.54	
		1.77	4.5	-	-	4.55	+1.10	4.17		-7.91	
		2.19	5.5	-	-	5.55	+0.90	5.00		-10.0	
		2.55	6.5	-	-	6.39	-1.72	5.69		-14.23	

[*a] "-" indicates that the corresponding equation is out of the validation limits (see Table 3 and 4)

a)

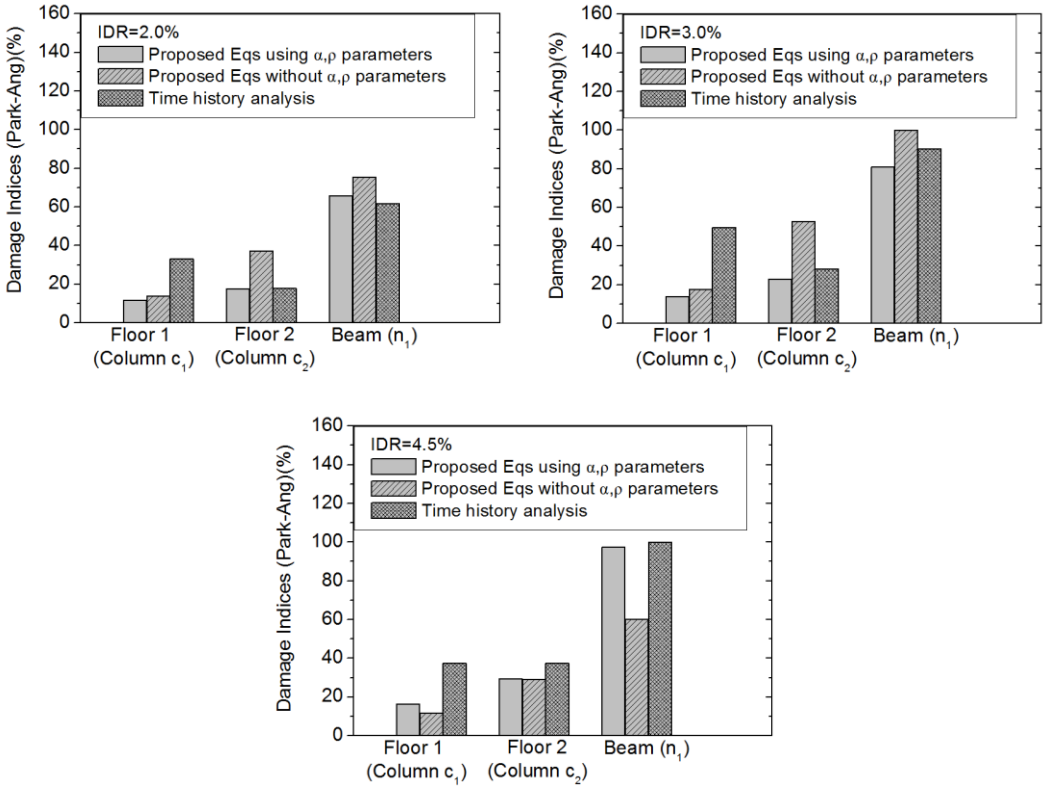

b)

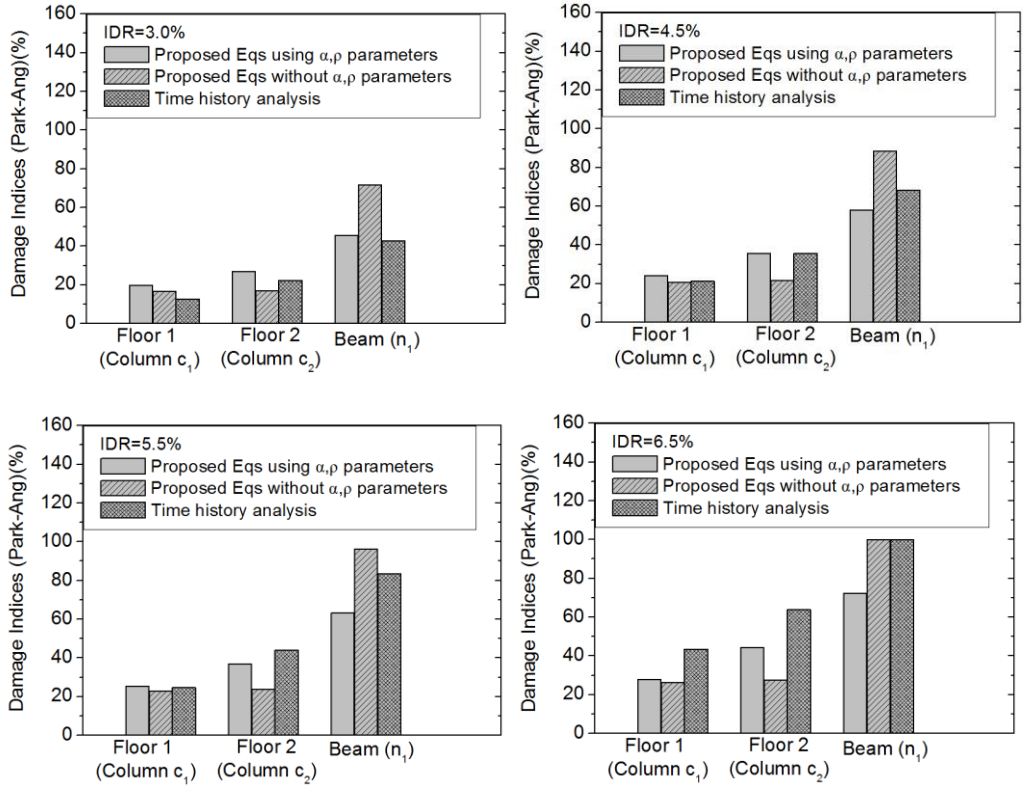

Figure 8: Values obtained by the proposed Eqs (12-23) versus values obtained by the time history analysis [27] for: a) soil type B and b) soil type D.

Based on Table 8, it can be seen that the proposed equations for IDR predict satisfactorily the target IDR_t even at very high inelastic response levels (i.e., for IDR larger than 4.0% according to SEAOC [10, 28] and Leelataviwat et al. (1999) [47]). In addition, as shown in Fig. 8(a) and Fig. 8(b), the proposed Eqs (12-14) and (18-20) estimate satisfactorily the wide range of the structural response, covering also the collapse level. On the other hand, the proposed Eqs (15-17) and (21-23) give a general view for the level of damage expected, which is very important at this preliminary phase of the design.

6. DISPLACEMENT/DAMAGE CONTROLLED DESIGN METHOD FOR PLANE CFT–MRFs WITH COMPOSITE BEAMS

In this section, the proposed displacement/damage controlled (DDC) seismic design method is described and used in conjunction with all the structural performance levels according to SEAOC [10, 28], i.e. Operational, Immediate Occupancy (IO), Life-Safety (LS), Near Collapse (NC) and Collapse (C), providing a wide range of values for every performance level according to FEMA [48] and ASCE [11]. These performance levels are depicted in Table 9, correlating their limit states in terms of IDR and DI with the earthquake design level. The general damage scale of Table 9 refers to individual members (beams and columns) and is associated with each performance level as recommend in [10, 28].

Table 9 summarizes the relationship between overall seismic performance and maximum inter-storey drift ratios, including also their related coefficient $S_a(T)$. Based on those performance levels, the concept of DDC is fully determined for a plane composite frame. The process of DDC design method is presented in Fig. 9 through a flowchart referring to Table 9. The proposed method is described step-by-step as follows:

1. Consider soil type, material and geometrical properties, number of building storeys (n_s), dead loads (G), live loads (Q), ground acceleration (A_g), behavior factor (q) and viscous damping ratio (ξ) as well as the design of the structure based on the response spectrum analysis or equivalent lateral loads per EC8 [9].
2. Set the structural performance level based on Table 9 and the predefined IDR of a considered structural performance level.
3. Scale-down or scale-up the $S_a(T)$ through the coefficient of $S_a(T)$ based on Table 9 and substitute its value into the proposed design equations for IDR (Eqs (3-9) and (7,8)).
4. Calculate a and ρ parameters and substitute them also into the proposed design equations for IDR. If the predefined IDR is not approximately equal to IDR_t, then iterate this process by setting other values of a and ρ. Otherwise, continue with the next step.
5. Check if the designed structure satisfies the other performance levels. Otherwise, redesign the structure and go again to step 4.

6. Apply the proposed expressions related to damage indices DI (Eqs (12-14) and (18-20)) as complementary to target inter-storey drift ratio (IDR) in order to evaluate the damage expected to the first storey, i.e. soft-storey collapse mechanism.

Table 9: Performance levels according to SEAOC [10, 28].

Structural Performance Levels (SPL)	Corresponding Interstorey Drift Ratios (IDRs)	Coefficient of Pseudo – Acceleration $S_a(T)$	Damage
Operational	≤ 0.5%	0.3	≤ 1%
Immediate Occupancy (IO)	≤ 1.8%	0.5	≤ 30%
Life-Safety (LS)	≤ 3.2%	1.0	≤ 60%
Near Collapse (NC)	≤ 4.0%	1.5	≤ 80%
Collapse (C)	> 4.0%	2.0	≤ 100%

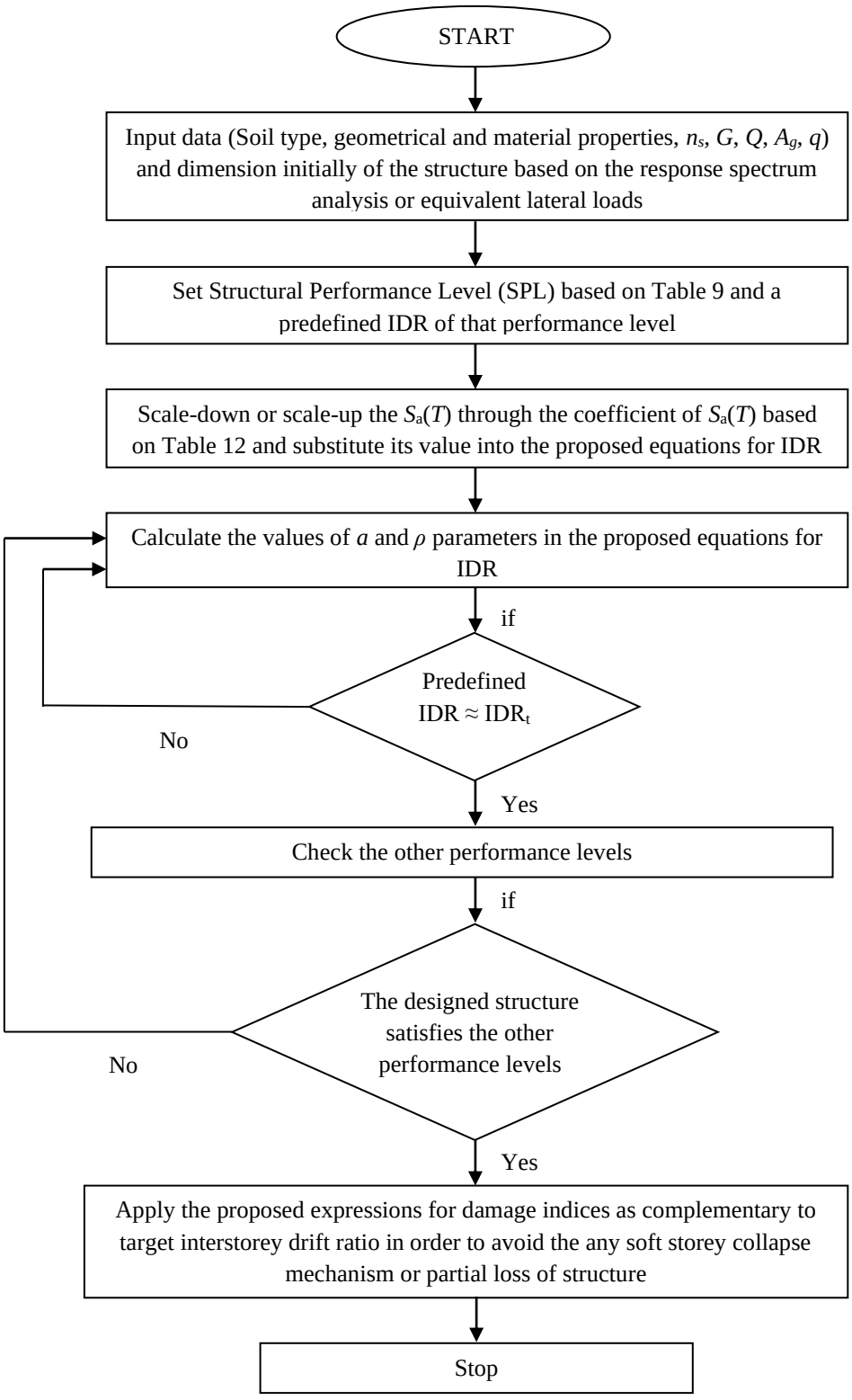

Figure 9: Flowchart for the DDC seismic design method based on the proposed equations.

6.1 Application of the displacement/damage controlled design to various performance levels

In this subsection, the proposed method is used for the design of the two examined frames of Table 7, in accordance with the design process of Fig. 9. It is noted that, these frames were designed for the *life safety* (LS) performance level based on EC8 [9]. The damage limitation is checked at a later step. The identified parameters a and ρ of the ten-storey building were found to be 0.130 and 1.793 respectively. By employing these values of a and ρ into Eq. (3), the target inter-storey drift ratio is estimated equal to IDR_t=2.09% and IDR_t=2.16%, respectively. These values are lower than 3.2% which is the drift limitation for life safety according to [10, 28]. The identified parameters a and ρ of the five storey building were found to be 0.456 and 0.987 respectively. By employing these a and ρ to Eq. (8), the target inter-storey drift ratio is estimated equal to IDR_t=2.84%. This value is also lower than 3.2%. The design of the two frames is now checked for the rest of the performance levels using the corresponding proposed equations for each performance level and soil type. Table 10 summarizes the results of the two designed frames where all performance levels are checked against the NLTH results.

Table 10: Displacement checking of the examined composite frames at all performance levels according to SEAOC [10, 28]: Parameters of soil type B: a=0.130, ρ=1.793 and parameters of soil type D: a=0.456, ρ=0.987.

Soil type	**n_s**	**T (sec)**	**Coefficient $S_a(T)$**	**$S_a(T)$ (g)**	**Performance Levels (SPL)**	**Limits for (IDRs)**	**IDR_{TH} (%)**	**IDR_t (%) Eq. (3)**	**IDR_t (%) Eq. (4)**	**Result**
B	10	1.521	0.3	0.112	Operational	≤ 0.5%	0.42	0.42	-	√
			0.5	0.187	Immediate Occupancy (IO)	≤ 1.8%	0.71	0.85	-	√
			1.0	0.374	Life-Safety (LS)	≤ 3.2%	1.97	2.16	-	√
			1.5	0.561	Near Collapse (NC)	≤ 4.0%	4.25	-[*a)]	4.10	x
			2.0	0.748	Collapse (C)	> 4.0%	7.27	-	5.89	√
			Coefficient $S_a(T)$	**$S_a(T)$ (g)**	**Performance Levels (SPL)**	**Limits for (IDRs)**	**IDR_{TH} (%)**	**IDR_t (%) Eq. (7)**	**IDR_t (%) Eq. (8)**	**Result**
D	5	0.760	0.3	0.320	Operational	≤ 0.5%	0.59	0.67	-	x
			0.5	0.533	Immediate Occupancy (IO)	≤ 1.8%	0.96	1.17	-	√
			1.0	1.067	Life-Safety (LS)	≤ 3.2%	2.19	-	2.84	√
			1.5	1.601	Near Collapse (NC)	≤ 4.0%	4.01	-	4.15	x
			2.0	2.134	Collapse (C)	> 4.0%	5.37	-	5.42	√

[*a] "-" indicates that the corresponding equation is out of the validation limits (see Table 3 and 4)

It can be seen in Table 10 that the proposed Eqs (4) and (8) for the 10-storey and 5-storey composite frames, respectively, provide larger values for the IDR_t than the limit values for the performance levels *near collapse* (NC) and *operational*, respectively. By comparing the results with those of NLTH analyses, one can conclude that all equations adequately estimated the exceedance of these performance level limit. The frame designs do not satisfy all the performance levels and therefore it is necessary to determine new

values for them. Table 11 shows the examined frames with larger section sizes in CFT columns and composite beams as well as the new values of a and ρ parameters based on the revised design.

Table 11: 10-storey and 5-storey CFT-MRFs based on the displacement/damage-controlled design: Geometric and material properties of the members, column to-beam strength ratio (a), beam-to-column stiffness ratio (ρ) and fundamental period of vibration (T).

n_s	Floors	CFT columns dimensions – material properties	Floors	Beams IPE	a	ρ	T (sec)	$S_a(T)$ (g)
10	1	(355.6x12.50)-40-235	1	300	0.201	1.611	1.512	0.376
	2-7	(406.4x6.30)-40-235	2-3	300				
			4-6	270				
			7	240				
	8-10	(355.6x6.00)-40-235	8	220				
			9	200				
			10	180				
5	1-2	(457x8.00)-40-235	1	270	0.460	0.779	0.801	1.066
			2	240				
	3-4	(406.4x6.30)-40-235	3	220				
			4	200				
	5	(355.6x6.00)-40-235	5	180				

As shown in Table 11, the identified parameters a and ρ of the ten storey building were found to be 0.201 and 1.611 respectively. By employing these values of a and ρ into Eq. (3), the target inter-storey drift ratio is estimated equal to IDR_t=1.93% and IDR_t=2.10%, respectively. These values are lower than 3.2% which is the drift limitation for life safety [10, 28]. The identified parameters a and ρ of the five storey building were found to be 0.460 and 0.779 respectively. By employing these a and ρ to Eq. (8) the target inter-storey drift ratio is estimated equal to IDR_t=2.17%. This value is lower than 3.2% too. Table 12(a) summarizes the results of this new design where all performance levels are checked against the NLTH analysis results. This time, IDR values for all performance levels do not exceed limit values.

Table 12(a): Displacement checking of the examined composite frames at all performance levels according to SEAOC [10, 28] for IDR: Parameters of soil type B: a=0.201, ρ=1.611 and parameters of soil type D: a=0.460, ρ=0.779.

Soil type	n_s	T (sec)	Coefficient $S_a(T)$	$S_a(T)$ (g)	Performance Levels (SP)	Limits for (IDRs)	IDR_{TH} (%)	IDR_t (%) Eq. (3)	IDR_t (%) Eq. (4)	Result
B	10	1.512	0.3	0.113	Operational	≤ 0.5%	0.40	0.41	-	√
			0.5	0.188	Immediate Occupancy (IO)	≤ 1.8%	0.69	0.82	-	√
			1.0	0.376	Life-Safety (LS)	≤ 3.2%	1.85	2.10	-	√
			1.5	0.565	Near Collapse (NC)	≤ 4.0%	3.85	-	4.00	√
			2.0	0.753	Collapse (C)	> 4.0%	7.14	-	5.78	√

			Coefficient $S_a(T)$	$S_a(T)$ (g)	Performance Levels (SP)	Limits for (IDRs)	IDR_{TH} (%)	IDR_t (%) Eq. (7)	IDR_t (%) Eq. (8)	Result
D	5	0.801	0.3	0.319	Operational	≤ 0.5%	0.55	0.49	-	√
			0.5	0.533	Immediate Occupancy (IO)	≤ 1.8%	0.92	0.97	-	√
			1.0	1.066	Life-Safety (LS)	≤ 3.2%	2.42	-	2.17	√
			1.5	1.598	Near Collapse (NC)	≤ 4.0%	3.82	-	3.16	√
			2.0	2.132	Collapse (C)	> 4.0%	5.03	-	4.13	√

Table 12(b): Damage checking of the examined composite frames at all performance levels according to SEAOC [10, 28] for damage indices: Parameters of soil type B: a=0.201, ρ=1.611 and parameters of soil type D: a=0.460, ρ=0.779.

Soil type	n_s	Coefficient $S_a(T)$	$S_a(T)$ (g)	Performance Levels (SPL)	Structural Damages	Damage of c_1 by TH analysis	Eq. (12)	Damage of c_2 by TH analysis	Eq. (13)	Damage of beam (n_1) by TH analysis	Eq. (14)
B	10	0.3	0.113	Operational	≤ 1%	0	4.07	0	5.66	12.98	24.14
		0.5	0.188	Immediate Occupancy (IO)	≤ 30%	0	5.59	1.75	8.25	21.78	35.42
		1.0	0.376	Life-Safety (LS)	≤ 60%	0	9.05	18.53	15.70	45.95	62.92
		1.5	0.565	Near Collapse (NC)	≤ 80%	1.68	12.42	40.42	25.05	82.87	91.36
		2.0	0.753	Collapse (C)	≤ 100%	7.00	15.87	78.7	36.90	137.27	121.78
	n_s	Coefficient $S_a(T)$	$S_a(T)$ (g)	Performance Levels (SPL)	Structural Damages	Damage of c_1 by TH analysis	Eq. (18)	Damage of c_2 by TH analysis	Eq. (19)	Damage of beam (n_1) by TH analysis	Eq. (20)
D	5	0.3	0.319	Operational	≤ 1%	0	8.25	0	7.74	0	19.19
		0.5	0.533	Immediate Occupancy (IO)	≤ 30%	0	10.14	1.73	10.43	8.39	26.15
		1.0	1.066	Life-Safety (LS)	≤ 60%	11	15.41	15.47	19.34	24.25	43.72
		1.5	1.598	Near Collapse (NC)	≤ 80%	15.12	18.61	28.35	25.47	43.80	56.86
		2.0	2.132	Collapse (C)	≤ 100%	20.60	20.77	41.23	29.81	65.82	67.37

According to Table 12(a), it can be seen that the revised design of the two frames following the proposed displacement/damage-controlled methodology meets successfully all the performance levels, leading also to a more economical design. It is also observed that the values of the proposed Eqs (3-4) and (7-8) are in agreement with those obtained by the time history analysis for the performance levels concerned. On the other hand, the proposed equations corresponding to *collapse* performance level provide a satisfactorily estimation of the expected IDR level.

Table 12(b) summarizes the estimated values of damage indices along with the time-history analysis results. It is observed that the proposed equations predict with fairly good accuracy, the damage indices from *life-safety* until *collapse* performance level. In general, it can be concluded that the proposed equations related to IDR_t give an adequate assessment regarding the damage-controlled design of the examined composite frames whereas the proposed equations related to damage indices act complementary for the designer to evaluate the potential of a soft-storey collapse mechanism at first floor or a partial loss of structure.

7. COMPARISON BETWEEN COMPOSITE MRFs AND STEEL MRFs

In this last section, a comparison between low-rise and medium-rise composite MRFs with CFT columns and composite beams and all-steel MRFs with HEB columns and IPE beams at various performance levels is conducted for the case of soil type B. The examined frames are composed of three-storeys and six-storeys with three bays. More specifically, the columns and the beams of the three-storey steel frame of [19] consist of standard HEB240 and IPE330 sections respectively, while its fundamental natural period is equal to 0.73 *sec*. On the other hand, the columns and the beams of the six-storey steel frame of [19] consist of standard HEB280 and IPE360 sections for the first four storeys and HEB260 and IPE330 for the last two storeys with fundamental natural period equal to 1.22 *sec*. In all cases, the frames are subjected to a vertical uniform load equal to 27.5 *kN/m* (dead and live load of floors) plus seismic load with PGA equal to 0.35*g*. Finally, in both types of frames, the height of each floor is equal to 3 *m* and the bay width is assumed to be 5 *m*, while the steel grade is S235.

The examined CFT-MRFs are investigated for soil type B, steel yield stress (f_y) and concrete compressive strength (f_c) equal to 235 and 40 *MPa*, respectively, and slab thickness equal to 15 *cm*. The design of those frames is based on Eurocode-3 [31], Eurocode-4 [32] and Eurocode-8 [9]. Table 13 presents the examined CFT frames (n_s) depicting among others the design of CFT frames, the parameters a and ρ, the fundamental period (T) and the pseudo-spectral acceleration ($S_a(T)$).

Table 13: CFT MRFs: Soil type, number of storey (n_s), geometric and material properties of the members, column to-beam strength ratio (a), beam-to-column stiffness ratio (ρ), fundamental period of vibration (T) and pseudo-spectral acceleration ($S_a(T)$).

Soil type	n_s	Floors	CFT columns dimensions – material properties	Floors	Beams IPE	a	ρ	T (sec)	$S_a(T)$ (g)
B	3	1-3	(355.6x6.0) – 40 – 235	1-3	240	0.328	2.051	0.565	1.007
	6	1-2	(559x10.0) – 40 – 235	1-2	240	0.805	0.361	0.949	0.600
		3-5	(406.4x6.30) – 40 – 235	3-4	220				
				5	200				
		6	(355.6x6.0) – 40 – 235	6	180				

The examined steel MRFs are compared with those of composite MRFs for inter-storey drift ratio and damage indices according to SEAOC [10, 28] at various performance levels. Table 14 presents the IDR_t for both composite and steel MRFs. In particular, the results of IDR_t for composite MRFs are obtained by the proposed Eq. (5), while the results of IDR_t for steel MRFs are obtained by employing the expressions proposed in [19] along with the associated results in terms of DI and IDR [19] for the various seismic hazard levels (i.e. frequently occurred earthquake (FOE), design basis earthquake (DBE), and maximum considered earthquake (MCE)). Accordingly, comparison is made related to the damage indices of those frames at beams and columns, as shown in Fig. 10. It should be noted that time-history analyses could be performed to extend the comparison of this section, however, the reliability of the adopted expressions

have been already validated by time-history analyses results increasing confidence of the present comparisons. This is also valid, because the expressions for steel and composite structures used here, have been developed on the basis of almost identical modeling assumptions and frame design characteristics allowing a direct comparison to be made focusing mainly on the different materials.

Table 14: Comparison of IDR_{max} for the composite and steel frames for various hazard and performance levels

Number of storeys (n_s)	HAZARD LEVELS	COMPOSITE FRAME		STEEL FRAME	
	Coefficient of $S_a(T)$	IDR_t	Performance Level	IDR_t	Performance Level
3	(DBE) 1.0	2.20%	Life-Safety	2.20%	Life-Safety
6	(FOE) 0.3	0.68%	Immediate Occupancy	0.58%	Immediate Occupancy
	(DBE) 1.0	1.80%	Immediate Occupancy	2.02%	Life-Safety
	(MCE) 1.5	3.10%	Life-Safety	3.23%	Near-Collapse

a)

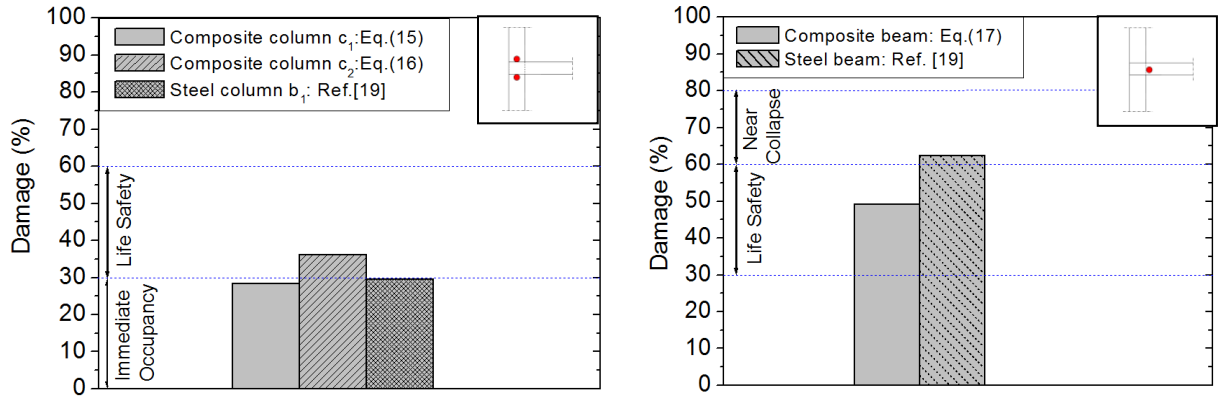

b)

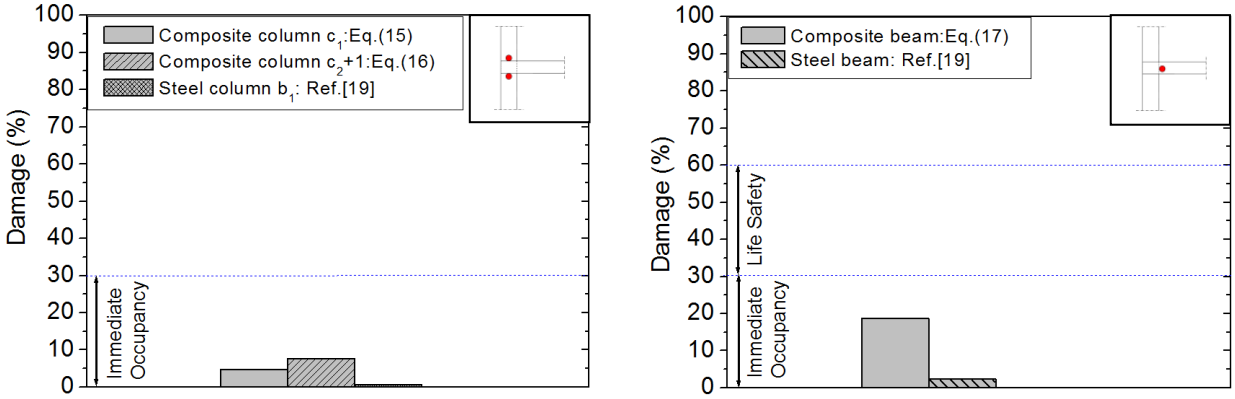

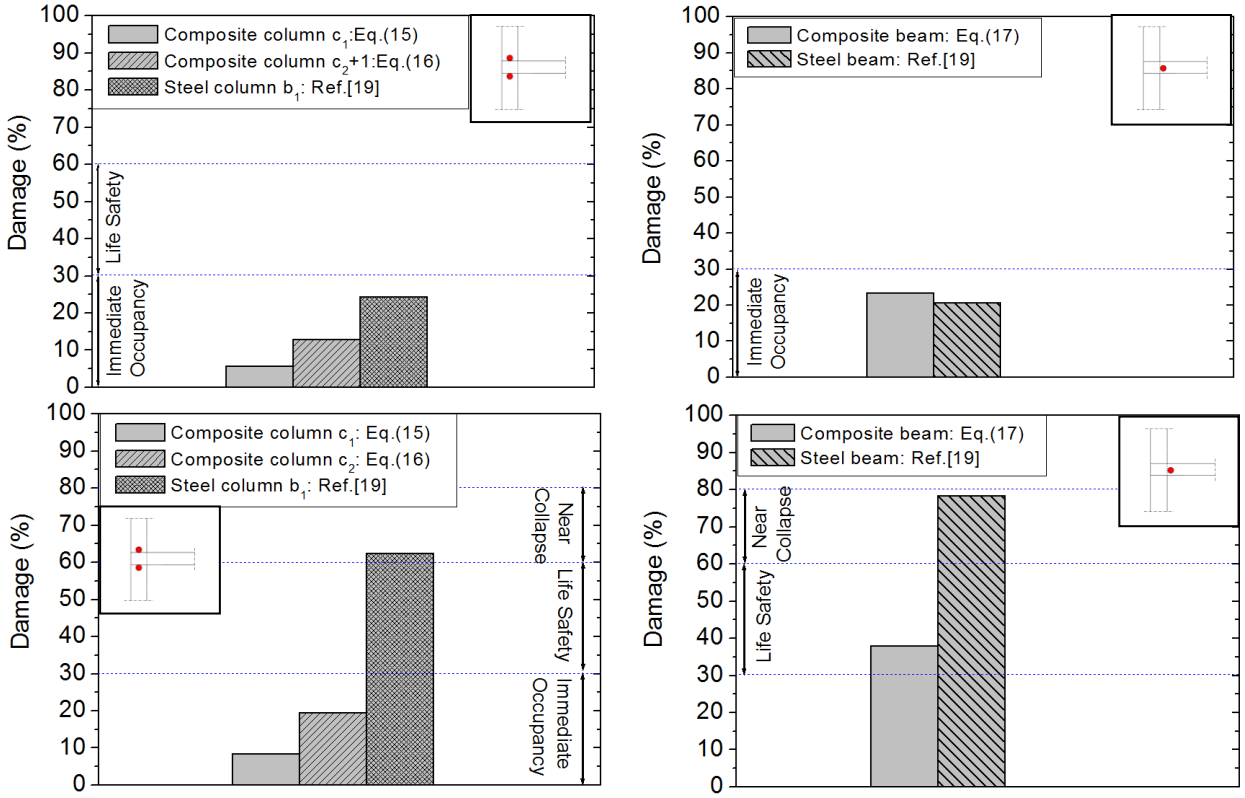

Figure 10: Composite column versus steel column and composite beam versus steel beam for: a) three storey buildings at performance level *life safety*, b) six storey buildings at performance levels *immediate occupancy*, *life safety* and *collapse* levels.

As shown in Table 14, comparing the IDR_t of the three-storey CFT-MRF and steel MRF for the hazard level DBE, it is observed that IDR_t fall within the same performance level, that of *life-safety*. In terms of IDR, a better performance is observed for the six-storey CFT-MRF than for the six-storey steel MRF because under the DBE and MCE hazard levels, a lower IDR is observed for the former frame than the latter one. More specifically, the CFT-MRF falls within the *immediate occupancy* and *life-safety* levels for the DBE and MCE hazard levels, respectively, while the all steel MRF falls within the *life-safety* and *near-collapse* levels for the corresponding hazard levels. In terms of local damage, the CFT-MRFs exhibit lower values particularly under the high hazard levels. As indicated in Fig. 10(a) for the three-storey buildings, while both type of columns fall within the *life-safety* performance level, the composite beam meets the *life-safety* criterion and the steel beam the *near-collapse* criterion. The low-damage behavior of composite members under consideration is confirmed in the six-storey buildings either under the DBE or the MCE hazard level. In some cases, the damage index for the CFT columns appeared to be less than half compared to the steel columns. Under MCE, both columns and beams fall within the *near-collapse* performance level in the steel MRF, while all members in CFT-MRFs are far below from the threshold of

life-safety. Compared to the CFT-MRF, a lower damage is observed for the steel MRF under the FOE hazard level. This might be related to the cracking of concrete that is expected in composite steel/concrete members under low seismic intensities. It is noted that this nonlinearity is explicitly considered in the modeling of CFT-MRFs either at composite columns or composite beams through the corresponding hysteretic models [37, 39]. Finally, in all cases the columns are stronger than beams, achieving the weak beam-strong column capacity design rule according to EC8 [9].

CONCLUSIONS

The seismic inelastic behavior of plane CFT-MRFs with composite beams founded on soil types B and D is investigated in this research study with the goal of establishing design equations. Based on extensive parametric studies, fairly broad response databanks are created, and empirical expressions are developed to estimate the inter-storey drift ratio (IDR) and structural damage indices (DI) at various performance levels. The developed expressions support the development of a displacement/damage controlled (DDC) seismic design method within the existing framework of current design codes. On the basis of the proceeding developments, the following conclusions can be stated:

1. A preliminary seismic design method can be performed for CFT-MRFs with composite beams through simple empirical expressions that integrate design parameters for the strength ratio (a) and the stiffness ratio (ρ) between columns and beams. The nonlinear time history analysis results revealed that the proposed expressions estimate the inelastic deformation demands (i.e., IDR and DI) for various earthquake intensities with a fairly good accuracy.

2. The proposed expressions, which take into account the parameters a and ρ predict more accurately the IDR and structural DI than the expressions that ignore these parameters. Nevertheless, the latter provide a very good view of the level of inelasticity excepted when a structure has not been sized yet and can be used much easier due to their simplicity. The use of the proposed expressions can significantly reduce the design iterations without response spectrum or nonlinear time history analyses. In addition, the proposed expressions related to DI can also be utilized to avoid any possible overall failure mechanism, e.g., soft-storey at the first floor, particularly for the low performance levels.

3. The proposed displacement/damage design expressions, in addition to helping the designer to dimension a structure, can also allow him to either directly determine the damage level for a given structure under a given seismic load, or determine the maximum seismic load a designed structure can sustain in order to exhibit a desired level of damage, thereby avoiding the execution of sophisticated nonlinear time-history analysis.

4. Comparing the CFT-MRFs and all steel MRFs for the design basis earthquake (DBE), the IDR of CFT-MRFs is similar with that of steel MRFs for the low-rise building. Similar behavior is also

observed for the DI of beams and columns with the composite beams to exhibit about 20% lower damage than the steel beams. The low-damage performance of CFT-MRFs is mainly demonstrated in the mid-rise building were both IDR and DI fall within lower performance levels compared to all steel MRFs for the same seismic intensity.

REFERENCES

[1] Hajjar JF (2002). Composite Steel and Concrete Structural Systems for Seismic Engineering. Journal of Constructional Steel Research; 58: 703-728.

[2] Varma AH, Ricles JM, Sause R, Lu LW (2002), Experimental Behavior of High Strength Square Concrete-Filled Steel Tube Columns. Journal of Structural Engineering of ASCE; 128(3): 309-318.

[3] Herrera RA, Ricles JM, Sause R (2008). Seismic Performance Evaluation of a Large-Scale Composite MRF Using Pseudodynamic Testing. Journal of Structural Engineering of ASCE; 134(2): 279-288.

[4] Skalomenos KA, Hatzigeorgiou GD, Beskos DE (2015). Modeling Level Selection for Seismic Analysis of Concrete-Filled Steel Tube/Moment-Resisting Frames by Using Fragility Curves. Earthquake Engineering & Structural Dynamics; 44(2): 199-220.

[5] Skalomenos KA, Hatzigeorgiou GD, Beskos DE (2018). Seismic Analysis and Design of Composite Steel/Concrete Building Structures Involving Concrete-Filled Steel Tubular Columns. in Recent Advances in Earthquake Engineering in Europe, 16th ECEE Thessaloniki, Greece, Pitilakis K (Editor), Springer Int. Publ., Cham, Switzerland, 387-411.

[6] Xiao LZ, Han LH, Lu H (2010). Concrete-Filled Tubular Members and Connections, Spon Press, New York.

[7] Skalomenos KA, Hatzigeorgiou GD, Beskos DE (2015). Seismic Behavior of Composite Steel/Concrete MRFs: Deformation Assessment and Behavior Factors. Bulletin of Earthquake Engineering; 13(12): 3871-3896.

[8] Elnashai AS, Broderick BM (1996). Seismic Response of Composite Frames—II. Calculation of Behaviour Factors. Engineering Structures; 18(9):707-723.

[9] European Committee of Standardization (2004). Eurocode 8: Design of Structures for Earthquake Resistance. Part 1: General Rules, Seismic Actions and Rules for Buildings. CEN, Brussels, EN 1998-1.

[10] Structural Engineers Association of California, SEAOC. Vision 2000 – A framework for Performance-Based Earthquake Engineering. Sacramento, CA; 1995.

[11] ASCE Standard ASCE/SEI 41-17. Seismic Evaluation of Retrofit of Existing Buildings. American Society of Civil Engineers, Reston, Virginia, USA; 2017.

[12] Chopra AK and Goel PK (2001). Direct Displacement-Based Design: Use of Inelastic vs. Elastic Design Spectra. Earthquake Spectra; 17(1): 47-63.

[13] Sullivan TJ, Calvi GM, Priestley MJN, Kowalsky MJ (2003). The Limitations and Performances of Different Displacement-Based Design Methods. Journal of Earthquake Engineering; 7(1): 201-241.

[14] Priestley MJN, Calvi MC, Kowalsky MJ (2007). Displacement-Based Seismic Design of Structures. IUSS Press, Pavia, Italy.

[15] Muho EV, Qian J, Beskos DE (2020). A direct displacement-based seismic design method using a MDOF equivalent system: application to R/C framed structures. Bulletin of Earthquake Engineering; 18: 4157-4188.

[16] Pian C, Qian J, Muho EV, Dimitri E. Beskos DE (2020). A hybrid force/displacement seismic design method for reinforced concrete moment resisting frames. Soil Dynamics and Earthquake Engineering; 129: doi.org/10.1016/j.soildyn.2018.09.002

[17] Tzimas AS, Karavasilis TL, Bazeos N, Beskos DE (2013). A Hybrid Force/Displacement Seismic Design Method for Steel Building Frames. Engineering Structures; 56: 1452-1463.

[18] Skalomenos KA, Hatzigeorgiou GD, Beskos DE (2015). Application of the Hybrid Force/Displacement (HFD) Seismic Design Method to Composite Steel/Concrete Plane Frames. Journal of Constructional Steel Research; 115: 179-190.

[19] Kamaris GS, Hatzigeorgiou GD, Beskos DE (2015). Direct Damage Controlled Seismic Design of Plane Steel Degrading Frames. Bulletin of Earthquake Engineering; 13(2): 587-612.

[20] Ayala AG, Castellanos H, Lopez S (2012). A Displacement-Based Seismic Design Method with Damage Control for RC Buildings. Earthquakes and Structures; 3(4): 413-434.

[21] Mehanny SSF and Deierlein GG (2001). Seismic Damage and Collapse Assessment of Composite Moment Frames. Journal of Structural Engineering; 127(9): 1045-1053.

[22] Song BI, Sezen H (2013). Experimental and Analytical Progressive Collapse Assessment of a Steel Frame Building. Engineering Structures; 56: 664-672.

[23] Yongtao B, Hongsong H, Jiantao W, Qing S (2017). Modeling on Collapse Behavior of High-Rise Concrete-Filled Steel Composite Frames Under Over-Design Seismic Excitations. Journal of Structure and Infrastructure Engineering; 13(12): https://doi.org/10.1080/15732479.2017.1303841

[24] Ghobarah A, Abou-Elfath H, Biddah A (1999). Response-Based Damage Assessment of Structures. Earthquake Engineering and Structural Dynamics; 28: 79-104.

[25] Villaverde R (2007). Methods to Assess the Seismic Collapse Capacity of Building Structures: State of the Art. Journal of Structural Engineering; 133 (1): 57-66.

[26] Kamaris GD, Skalomenos KA, Hatzigeorgiou GD, Beskos DE (2016). Seismic Damage Estimation of In-Plane Regular Steel/Concrete Composite Moment Resisting Frames. Engineering Structures, 115; 67-77.

[27] Carr AJ (2008). Inelastic Time-History Analysis of Two-Dimensional Framed Structures. Department of Civil Engineering, University of Canterbury, New Zealand.

[28] Structural Engineers Association of California (SEAOC) (1999). Recommended Lateral Force Requirements and Commentary "Blue Book". Structural Engineers Association of California, 7th Edition Sacramento, CA.

[29] Serras DN (2019). Controlled Damage Based Design of Composite Structures Under Seismic Loading. PhD thesis, School of Sciences and Technology, Hellenic Open University, Patras, Greece.

[30] Chopra AK (2007). Dynamics of Structures. Pearson Prentice Hall, Upper Saddle River, New Jersey, USA.

[31] European Committee of Standardization (2009). Eurocode 3: Design of Steel Structures-Part 1.1: General Rules and Rules for Buildings. EN 1993-1, CEN, Brussels, Belgium.

[32] European Committee of Standardization (2004). Eurocode 4: Design of Structures for Earthquake Resistance. Part 1: General Rules, Seismic Actions and Rules for Buildings. EN 1998-1, CEN, Brussels, Belgium.

[33] SAP2000 (1995): Analysis Reference, Structural and Earthquake Engineering Software, Computer and Structures, Version 15, Inc., Berkeley.

[34] DEV-C++ (2015). Bloodshed Software-Providing Free Software to the Internet Community.*bloodshed.net*.

[35] Hatzigeorgiou GD (2008). Numerical Model for the Behavior and Capacity of Circular CFT Columns. Part II: Verification and extension. Engineering Structures; 30(6): 1579-1589.

[36] Serras DN, Skalomenos KA, Hatzigeorgiou GD, Beskos DE (2016). Modeling of Circular Concrete-Filled Steel Tubes Subjected to Cyclic Loading. Structures; 8(1): 75-93.

[37] Serras DN, Skalomenos KA, Hatzigeorgiou GD, Beskos DE (2017). Inelastic Behavior of Circular Concrete-Filled Steel Tubes: Monotonic Versus Cyclic Response. Bulletin of Earthquake Engineering, 5413-5434.

[38] Al-Bermani FGA, Li B, Zhu K, Kitiponchai S. (1994). Cyclic and Seismic Response of Flexibility Jointed Frames. Engineering Structures; 16: 249-55.

[39] Skalomenos KA, Hatzigeorgiou GD, Beskos DE (2014). Parameter Identification of Three Hysteretic Models for the Simulation of the Response of CFT Columns to Cyclic Loading. Engineering Structures; 61: 44-60.

[40] Amadio C, Bedon C, Fasan M, Pecce MR (2017). Refined Numerical Modeling for the Structural Assessment of Steel-Concrete Composite Beam-To-Column Joints Under Seismic Loads. Engineering Structures; 138: 394-409.

[41] Farghaly AA (2013). Parametric Study on Equivalent Damping Ratio of Different Composite Structural Building Systems. Steel and Composite Structures; 14(4): 349-365.

780 [42] Lam N, Wilson J, Hutchinson G (1998). The Ductility Reduction Factor in the Seismic Design of the
781 Buildings. Earthquake Engineering Structures Dynamics; 27: 749-769.
782 [43] Hatzigeorgiou GD (2010). Behavior Factors for Nonlinear Structures Subjected to Multiple Near-
783 Fault Earthquakes. Computers and Structures; 88(5-6): 309-321.
784 [44] Park Y, Ang AH (1985). Mechanistic Seismic Damage Model for Reinforced Concrete. Journal of
785 Structural Engineering-ASCE; 111(3): 722-39.
786 [45] Loulelis D, Hatzigeorgiou GD, Beskos DE (2012). Moment Resisting Steel Frames under Repeated
787 Earthquakes. Earthquake and Structures; 3(3-4): 231-248.
788 [46] Hatzigeorgiou GD, Liolios AA (2010). Nonlinear Behavior of RC Frames Under Repeated Strong
789 Ground Motions. Soil Dynamics and Earthquake Engineering; 30: 1010-1025.
790 [47] Leelataviwat S, Goel SC, Stojadinović B (1999). Towards Performance-Based Seismic Design of
791 Structures. Earthquake Spectra; 15(3): 435-461.
792 [48] FEMA (1997). FEMA-273 Building Seismic Safety Council, NEHRP Guidelines for the Seismic
793 Rehabilitation of Buildings, Federal Emergency Management Agency, Washington (DC).